

1 **Enabling a process-oriented hydro-biogeochemical model to simulate soil**
2 **erosion and nutrient losses**

3 Siqi Li ^{1, 2, 3}, Bo Zhu ⁴, Xunhua Zheng ^{1, 5}, Pengcheng Hu ⁴, Shenghui Han ¹, Jihui Fan ⁴, Tao
4 Wang ⁴, Rui Wang ¹, Kai Wang ¹, Zhisheng Yao ¹, Chunyan Liu ¹, Wei Zhang ^{1,*}, Yong Li ^{1,*}

5 ¹ State Key Laboratory of Atmospheric Boundary Layer Physics and Atmospheric Chemistry,
6 Institute of Atmospheric Physics, Chinese Academy of Sciences, Beijing 100029, China

7 ² Institute of Carbon Neutrality, Qilu Zhongke, Jinan 250100, China

8 ³ State Environmental Protection Key Laboratory of Formation and Prevention of Urban Air
9 Pollution Complex, Shanghai Academy of Environment Sciences, Shanghai 200233, China

10 ⁴ Institute of Mountain Hazards and Environment, Chinese Academy of Sciences, Chengdu
11 610041, China

12 ⁵ College of Earth and Planetary Science, University of Chinese Academy of Sciences, Beijing
13 100049, China

14 * Corresponding author

15 Tel.: +86 10 13681042146

16 +86 10 13107488562

17 E-mail address: zhangwei87@mail.iap.ac.cn (W. Zhang)

18 yli@mail.iap.ac.cn (Y. Li)

19

20 **Abstract**

21 Water-induced erosion and associated particulate carbon (C), nitrogen (N) and phosphorus
22 (P) nutrient losses were the vital parts of biogeochemical cycling. Identifying their intensity
23 and distribution characteristics is of great significance for the control of soil and water loss
24 and N/P nonpoint source pollution. This study incorporated the modules of physical soil
25 erosion and the particulate C, N and P losses into the process-oriented hydro-biogeochemical
26 model (Catchment Nutrients Management Model coupled Denitrification-Decomposition,
27 CNMM-DNDC) to enable it to predict soil and water loss. The results indicated that the
28 upgraded CNMM-DNDC i) performed well in simulating the observed temporal dynamics
29 and magnitudes of surface runoff, sediment and particulate N/P losses in the lysimetric plot
30 of the Jieliu catchment in Sichuan Province; ii) successfully predicted the observed monthly
31 dynamics and magnitudes of stream flow, sediment yield and particulate N losses at the
32 catchment outlet, with significant univariate linear regressions and acceptable Nash–Sutcliffe
33 indices higher than 0.74. The upgraded CNMM-DNDC demonstrated that more proportion
34 of the particulate N to total N during the period with large precipitations than that during the
35 droughty period (16.2%–26.6% versus 2.3%–12.4%). The intensities of soil erosion and
36 particulate nutrient losses in the Jieliu catchment was closely related to land use type in the
37 order of sloping cultivated cropland > residential area > forest land. The scenario analysis
38 demonstrated that high greenhouse gas (GHG) emissions scenarios provided a greater risk of
39 soil erosion than did low GHG emissions scenarios and land use change (i.e., from the
40 sloping upland to forest land) could help to mitigate soil and water loss accelerated by

41 climate change in the future. The upgraded model was demonstrated to have the capability of
42 predicting ecosystem productivity, hydrologic nitrogen loads, emissions of GHGs and
43 pollutant gases, soil erosion and particulate nutrient losses, which renders it a potential
44 decision support tool for soil erosion and nonpoint source pollution control coordinated with
45 increasing production and reducing GHGs and pollutant gases emissions in a catchment.

46 **Keywords**

47 CNMM-DNDC, ROSE, soil erosion, particulate carbon/nitrogen/phosphorus loss

48 **1. Introduction**

49 Water-induced erosion and associated particulate carbon (C), nitrogen (N) and phosphorus
50 (P) nutrient losses are among the primary threats leading to the decline in soil fertility and the
51 increases in land degradation, channel sedimentation and eutrophication of downstream rivers
52 and lakes (Berhe et al., 2018; Ekholm and Lehtoranta, 2012; Garcia-Ruiz et al., 2015). This
53 global environmental issue are becoming serious (Ma et al., 2021; Yang et al., 2003). A
54 previous study found that the vulnerability of water-induced erosion increased over 51% of the
55 global surface from 1982 to 2015 (Liu et al., 2019). Climate change and anthropogenic
56 activities (such as land use change) are the two principal driving forces that have complicated
57 and altered the hydrological cycle and water-induced erosion during recent decades (Piao et al.,
58 2007; Zeng et al., 2015).

59 Quantitative assessments of the water-induced soil erosion intensity and identification of
60 its temporal and spatial distribution characteristics are of great importance for preventing soil
61 and water loss and have attracted the attention of researchers (e.g., Jetten et al., 2003; Jiang et
62 al., 2017; Panagos et al., 2015c). Lysimetric plot experiments have been developed as a direct

63 field measurement method for the accurate quantification of surface runoff and water-induced
64 erosion (e.g., Kosmas et al., 1997; Sumner et al., 1996; Zhu et al., 2009). However, the in situ
65 field measurements of water-induced soil erosion with high cost of labor and money can only
66 cover a small piece of the sampling units. It is unrealistic to expect direct field measurements
67 to quantify water-induced erosion everywhere under various conditions.

68 Simulations of mathematical models are likely to compensate for the deficiency of direct
69 field measurements on soil erosion. The Universal Soil Loss Equation (USLE, Wischmeier and
70 Smith, 1978), its revised version (RUSLE) (Renard et al., 1997) and its modified version
71 (MUSLE) (Williams 1975) have been developed into widely used empirical mathematical
72 models to directly calculate soil erosion based on rainfall, soil property, topography, cover and
73 management data. The USLE or RUSLE quantify only the various influencing factors that
74 impact the soil loss associated with soil erosion, which is not directly related to the process of
75 surface runoff and does not involve the specific process of sediment transport yet (Donovan,
76 2022; Meinen and Robinson, 2021). Fortunately, the physical process-based ROSE model
77 named after the name of developer (Rose et al., 1983) conceptualizes the soil erosion process
78 by conceiving three continuous and simultaneous physical processes, including rainfall
79 detachment, sediment entrainment and sediment deposition, thus providing good performance
80 in estimating sediment yield at the plot scale. However, the ROSE model focuses only on the
81 physical processes of water-induced erosion without engaging the C and N cycles of the
82 ecosystem. The Soil and Water Assessment Tool (SWAT) (Arnold et al., 1998), a semi
83 distributed hydrological model, incorporates the USLE or MUSLE to predict soil erosion at the

84 level of hydrological response units, in which the routing of sediment transportation is not
85 considered and the modeling of the biogeochemical element cycle is relatively simple and
86 empirical (Ferrant et al., 2011; Pohlert et al., 2007). However, the transport of particulate C, N,
87 and P nutrients accompanied by water-induced erosion crucially depends on the C and N cycles
88 of ecosystems in a catchment. Previous research demonstrated that the C, N, and P contents in
89 the eroded soil were richer than that in the surface soil, which usually applied the elemental
90 enrichment module to predict (Sharply, 1980). Therefore, knowledge of the coupling between
91 the process-oriented hydro-biogeochemical model combined with the complex C and N cycles
92 and the soil erosion model based on physical processes (e.g., ROSE) is essential to accurately
93 predict soil erosion and associated particulate C, N, and P nutrient transport. A recently
94 developed hydro-biogeochemical model (CNMM-DNDC) by Zhang et al. (2018) might
95 become a realistic tool that can be used to address the abovementioned problem. The
96 CNMM-DNDC model introduces the complex C and N biogeochemical modules (including
97 the modules of decomposition, nitrification, denitrification and fermentation) of a widely used
98 biogeochemical model (DeNitrification-DeComposition model, DNDC, Li et al., 1992) into the
99 distributed hydrological framework of the Catchment Nutrients Management Model (CNMM,
100 Li et al., 2017). The adsorption–desorption, immobilization, transposition of P element of the
101 CNMM-DNDC model were originated from CNMM. The CNMM-DNDC model has been
102 used to conduct a comprehensive simulation of the complex hydrological and biogeochemical
103 processes (such as ecosystem productivity, hydrologic N loads, gaseous N losses and
104 greenhouse gas emissions) of a subtropical catchment with various landscapes (Zhang et al.,

105 2018), a model evaluation of nitrous oxide (N₂O) and nitric oxide (NO) emissions from a
106 subtropical tea plantation (Zhang et al., 2020b), a model evaluation and regional simulation of
107 nitrate leaching in the black soil region of Northeast China (Zhang et al., 2021a) and a
108 comprehensive model modification and evaluation of NH₃ volatilization from fertilized
109 croplands (Li et al., 2022b). However, the CNMM-DNDC model still lacks the capacity to
110 simulate the processes of soil erosion and associated particulate C, N, and P nutrient
111 transportation.

112 Therefore, we hypothesize that the accurate simulation of soil erosion and associated
113 particulate C, N, and P nutrient losses can be realized by incorporating the soil erosion physical
114 model and the element enrichment module into the process-oriented hydro-biogeochemical
115 model with complex C and N cycles. Based upon the above hypothesis, the objectives of this
116 study were to i) introduce the ROSE model (a physical soil erosion model) and the enrichment
117 module of the particulate nutrients into the hydrological process of the CNMM-DNDC model;
118 ii) evaluate the performance of the CNMM-DNDC model in simulating the temporal and
119 spatial distributions of soil erosion and associated particulate C, N, and P transportation at the
120 plot and catchment scales; and iii) investigate the impact of climate change and human
121 activities (such as land use change) on the losses of soil and particulate nutrients.

122 **2. Materials and methods**

123 **2.1 Catchment description**

124 The Jieliu catchment (31°16'N, 105°28'E, 400–600 m a.s.l.), located in Sichuan Province
125 of Southwest China (Zhu et al., 2009), was used for the model calibration and validation. This
126 catchment is situated in the upper reaches of the Yangtze River and has a typical subtropical

127 monsoon climate. During the period from 2005 to 2018, the annual mean temperature was
128 16.7 °C, and the average annual precipitation was 720 mm, 75% of which occurred during the
129 period between June and September (<http://yga.cern.ac.cn>). The soil in the catchment is
130 dominated by Calcaric purple soil, classified as a Pup-Orthic Entisol in the Chinese Soil
131 Taxonomy or as an Entisol classified in the U.S. Soil Taxonomy (Zhu et al., 2009). The total
132 area of the Jieliu catchment is approximately 35 ha, and it is dominated by sloping croplands
133 (58%), forest lands (31%) and the village residential areas (10%). The primary crops cultivated
134 in the sloping croplands are maize (*Zea mays* L.), winter wheat (*Triticum aestivum* L.), rape
135 (*Brassica napus* L.) and rice (*Oryza sativa* L.). The N, P and potassium (K) fertilizers are
136 applied at rates of 130–330 kg N ha⁻¹ yr⁻¹ (ammonium bicarbonate or urea), 72–162 kg P ha⁻¹
137 yr⁻¹ (calcium superphosphate) and 45–68 kg K ha⁻¹ yr⁻¹ (potassium chloride), respectively
138 (Zhang et al., 2018). Four replicate lysimetric plots (an area of 8 m by 4 m with a slope
139 gradient of 7%, Fig. 1) were set to measure the surface runoff and the losses of the particulate
140 N and P (Zhu et al., 2009). To avoid unexpected seepage, each lysimetric plot was
141 hydrologically isolated with the cement-filled partition walls, which was inserted at least 60 cm
142 deep into the bedrock. A conflux trough with a bucket was built at the topsoil to collect the
143 surface runoff flow (Zhu et al., 2009).

144 **2.2 Overview of the CNMM-DNDC model**

145 The CNMM-DNDC is a process-oriented hydro-biogeochemical model, which was
146 established following the basic physics, chemistry and biogeochemistry theories, through
147 incorporating the processes of C and N cycling of the DNDC into the hydrological framework

148 of the CNMM (Zhang et al., 2018). The core processes simulated by CNMM-DNDC include
149 thermal conduction, energy balance, hydraulic dynamics (e.g., soil evaporation, transpiration,
150 canopy interception, infiltration, percolation, surface runoff, subsurface flow and water uptake
151 by plants), C and N cycling (e.g., mineralization, immobilization, decomposition, nitrification,
152 denitrification, nitrate leaching, urea hydrolysis, plant uptake, and gas emissions), plant growth
153 (e.g., photosynthesis and respiration) and the discharge and water quality of the river-networks
154 (Fig. S1).

155 **2.3 Model modifications**

156 The CNMM-DNDC model can simulate the lateral movements of water-soluble nutrients
157 (e.g., ammonium, nitrate, phosphate and dissolved organic matter) by surface and subsurface
158 runoff, whereas it lacks the capabilities of simulating soil erosion and sediment transport
159 caused by surface runoff and the associated transportation of particulate C, N, and P. To
160 address such a deficiency, this study incorporated the modules of soil erosion and element
161 enrichment into the lateral hydrological framework of the CNMM-DNDC model (Text S1).
162 Therefore, the upgraded CNMM-DNDC model was equipped with the ability to estimate the
163 movements of soil particles and particulate nutrients transported with surface runoff in the
164 lateral dimension (Fig. S1). The soil erosion module adopted the simplified ROSE model (Rose
165 et al., 1983; Stewart, 1985), which is a process-oriented soil erosion model. The ROSE model
166 is based on the dynamic equilibrium of three simultaneous processes, including rainfall
167 detachment, runoff detachment, and sediment deposition. In an individual erosion event, the
168 process of runoff detachment dominates, and the latter two processes of rainfall detachment

169 and sediment deposition can be generally neglected (Stewart, 1985). Therefore, in the
170 simplified ROSE module, the sediment yield (Y_s , kg dry soil ha⁻¹) resulting from soil erosion
171 was driven by the actual surface runoff (R_s , m) and concomitantly regulated by the coverage
172 fraction of vegetation (C_v , fraction) and the land's slope angle, which was represented by the
173 absolute value of the sine value of the land's slope angle (S_i , dimensionless), as shown by Eq.
174 (1). The complete physical processes for soil erosion of the ROSE module (Text S2) was the
175 reason why we chose it though the two processes which had minor effects on soil erosion in an
176 individual erosion event were neglected in the simplified ROSE module. The upgraded
177 CNMM-DNDC was expected to provide the effects of the field managements (e.g., tillage) on
178 soil chemical or physical properties to influence soil erosion instead of applying the empirical
179 mathematical formula to predict the effects of the field managements like what the USLE and
180 its revised or modified versions did (Panagos et al., 2015b; Meinen and Robinson, 2021).

$$Y_s = 27 \times 10^6 (1 - C_v) \eta S_i R_s \quad (1)$$

181 Where R_s is calculated from the existing hydrological module of the CNMM-DNDC
182 model, in which R_s occurs in the following two cases. First, R_s is caused by the mechanism of
183 excess infiltration, in which the water input (i.e., precipitation and irrigation) is greater than the
184 maximum infiltration capacity of the soil. Second, R_s is derived from the mechanism of excess
185 storage, in which precipitation or irrigation still occurs when the soil surface water content
186 exceeds the corresponding saturated water content. The direction of the surface runoff conflux
187 is estimated by the distributed weights of four neighboring grids (i.e., in the upper, lower, left

188 and right directions), which are calculated based on the elevation of these grids. η
189 (dimensionless) is referred to as the efficiency of sediment entrained by surface runoff, which
190 depends on soil texture and C_v , as shown in Eq. (2).

191 .

$$\eta = a_1 e^{-0.15C_v} \quad (2)$$

192 In Eq. (2), a_1 is referred to as the rate of sediment carried by surface runoff on bare land,
193 which differs for various soil textures and generally needs to be calibrated by the observed data
194 of sediment loss for a given study area. Loch and Donnollan (1983) reported that a_1 varies
195 from 1.0% to 8.7% in Middle Ridge clay loam and Irving clay soils. Among the only eight soil
196 erosion observations conducted in the lysimetric plot from 2015 to 2017, four observations in
197 2016 were provided for model calibration. More soil erosion observation of the lysimetric plots
198 with different soil textures were needed to operate the CNMM-DNDC to establish the general
199 relationship between the a_1 and soil texture (e.g., soil clay, silt and sand contents) in future.
200 Moreover, the value of C_v for the natural vegetation (e.g., forest and grass) was addressed as
201 half of the ratio of the real leaf area index (LAI) and the maximum LAI (which is one of the
202 model inputs). For the crop system, the LAI was the function of the growing index, which is
203 estimated by the ratio of the accumulated temperature from sowing to the present time to the
204 accumulated thermal degree for maturity in the plant growth module. So the C_v value of the
205 crop was calculated by the growing index. The C_v value of the artificial lands (e.g., the urban or
206 rural residential areas) was calibrated and set to 0.1, which represented the effects of concrete

207 roads and residential buildings on the reduction of the soil area exposed to erosion. The C_v
208 value of the artificial lands might be generally quantified using the coverage of building and
209 cement roads according to more observations in future.

210 It is known that the C, N, and P elements of the eroded sediments are usually richer than
211 those of the in situ soils from which the eroded sediments originate (Massey and Jackson, 1952;
212 Schiettecatte et al., 2008; Wan and El-Swaify, 1998). The above phenomenon is usually
213 referred to as sediment enrichment, which can be quantified by an empirically based
214 enrichment ratio (E). E is usually defined as the ratio of the concentration of C, N, and P
215 elements in the eroded sediment to that in the source soil (Sharpley, 1980; Teixeira and Misra,
216 2005). Generally, as more eroded sediment is produced, the richness of the C, N, and P
217 elements decreases. The enrichment ratio of the C and N nutrients (E_{CN}) is estimated by Eq. (3),
218 which was adapted from McElroy et al. (1976) and Williams and Hann (1978). The
219 pre-exponential factor (k_1) of Eq. (3) was calibrated to 1.2 using the particulate N data
220 observed at the lysimetric plot in this study. The enrichment ratio of P nutrients (E_P) is
221 calculated by Eq. (4) cited from Sharpley (1980).

$$E_{CN} = k_1(Y_s \times 10^{-4})^{-0.2468} \quad (3)$$

$$E_P = e^{(2.46 - 0.2 \log Y_s)} \quad (4)$$

222 The yields of particulate C (P_C , kg C ha⁻¹), N (P_N , kg N ha⁻¹), and P (P_P , kg P ha⁻¹)
223 nutrients caused by soil erosion were calculated based on E , Y_s and the content of the
224 corresponding organic C (C_C , g C ha⁻¹), N (C_N , g N ha⁻¹), and P (C_P , g P ha⁻¹) pools in topsoil

225 using Eqs. (5–7), respectively. BD (g m^{-3}) and D_s (m) refer to the soil bulk density and the
226 depth of topsoil, respectively. Eight of the soil organic C and N subpools participated in the
227 process of soil erosion, including the pools of very labile, labile, and resistant decomposable
228 litters, labile and resistant active microbes, labile, resistant and passive humus, whereas five of
229 the soil organic P subpools were involved in the process of soil erosion, including the pools of
230 active and passive organic P, active and dead microorganism P, and inert stable P. Meanwhile,
231 the flows of C, N and P among the pools of the labile and resistant organic and inorganic were
232 considered in the CNMM-DNDC. For example, the C and N of the litter and humus pools and
233 the P of the pools of the active or passive organic P and the inert stable P could flow into
234 inorganic pools and the microbe pools by decomposition. The particulate C, N, and P losses
235 calculated by the element enrichment module were also deducted from the corresponding
236 subpools of the topsoil. Subsequently, the eroded soil and the particulate C, N, and P nutrients
237 are transported with surface runoff and eventually drain into streams. The upgraded model
238 considered the mass balances of soil water and the elements of C, N, and P, without
239 considering soil body balance.

$$P_C = \sum_{i=1}^8 \frac{10^{-7} E_{CN} C_{C_i} Y_s}{BD \cdot D_s} \quad (5)$$

$$P_N = \sum_{j=1}^8 \frac{10^{-7} E_{CN} C_{N_j} Y_s}{BD \cdot D_s} \quad (6)$$

$$P_P = \sum_{k=1}^5 \frac{10^{-7} E_P C_{P_k} Y_s}{BD \cdot D_s} \quad (7)$$

240 **2.4 Preparation for model simulation**

241 The input data for driving the model operation consisted of the meteorological data at the
242 3-hour scale (including average air temperature, solar radiation, long wave radiation, wind
243 speed, humidity and total precipitation), the spatialized soil properties (including soil texture,
244 soil organic carbon, bulk density and pH), the gridded digital elevation model (DEM, Fig. 1)
245 with a resolution of 5 m × 5 m, the spatial distribution of land use (Fig. 1) and cropping
246 systems, and the field management practices. Taking the efficiency of the model calculation
247 and the accuracy of the biogeochemical process description into consideration, the upgraded
248 CNMM-DNDC model conducted a simulation with a grid of 15 m × 15 m from 2004 to 2017,
249 with an initial spin-up period of ten years. The DEM, soil properties, land use, cropping
250 systems, field management practices and meteorological data from 2004 to 2014 were
251 primarily adapted from Zhang et al. (2018). The remaining meteorological data were adapted
252 from the hourly observations provided at the National Science & Technology Infrastructure
253 (<http://rs.cern.ac.cn>). The information about the vertical layered soil properties (e.g., soil bulk
254 density, pH, clay content, field capacity, wilting point, saturated hydraulic conductivity, organic
255 C, and total N and P contents) of different land uses were listed in Table S1. The input data of
256 soil properties, DEM, land use, cropping systems, and field management practices were
257 resampled to the ASCII grids with a resolution of 15 m × 15 m using the ArcGIS 10.0 software
258 package (ESRI, Redland, CA, USA). The observation data measured at the lysimetric plot and
259 the catchment outlet, which were listed in Table S2, contributed to model calibration and
260 validation. The surface runoff, associated sediment yield, and particulate and total N losses

261 from 2004 to 2006 with three replicates and the surface runoff, associated sediment yield, and
262 total P loss from 2017 to 2018 with three replicates measured at the lysimetric plots were
263 adapted from Deng et al. (2011) and Hu (2020), respectively. The monthly stream flow,
264 sediment yield, and particulate and total N losses from 2007 to 2008 measured at the catchment
265 outlet were directly cited from Deng et al. (2011). Total N referred to the total amount of NH_4^+ ,
266 NO_3^- , dissolved organic N and particulate N. Total P referred to the total amount of dissolved
267 organic and inorganic P and particulate P. Among them, the observed data from the lysimetric
268 plot in 2004 (with seven observation times) and 2016 (with four observation times and a heavy
269 precipitation event) and the observed data from the catchment outlet in 2007 were used for
270 model calibration, and the remaining observed data were used for model validation. Previously,
271 a comprehensive and systematic verification of the CNMM-DNDC simulation on soil
272 temperature, soil moisture, crop yield, water flows, nitrate loss, fluxes of methane, ammonia,
273 NO and N_2O , and stream discharges of water and NO_3^- had been conducted by Zhang et al.
274 (2018), which performed statistically in good agreement with the observations.

275 **2.5 Climate and land use scenario settings**

276 Scenario analysis was adopted to assess the impact of climate change and land use change
277 on water-induced erosion and its accompanying nutrient losses. The baseline scenario was set
278 as the traditional land use types and managements in 2008 (the year for model validation) with
279 local and historical meteorology. Two groups of climate change and land use change scenarios
280 were designed: single-factor change and multifactor change scenarios (Table S3). The
281 single-factor change scenarios altered only one factor while keeping the others constant. The

282 single-factor change scenarios of climate change consisted of two parts. One part for air
283 temperature change was altered within the range of $-4\text{ }^{\circ}\text{C}$ to $+4\text{ }^{\circ}\text{C}$ with an interval of $0.2\text{ }^{\circ}\text{C}$.
284 The other part for precipitation change was altered by the range from -30% to $+30\%$ with an
285 interval of 2% . For the sake of argument, we divided air temperature and precipitation
286 single-factor scenarios into four groups: lower and higher warming group (i.e., air temperature
287 increased from 0°C to 2°C and from 2°C to 4°C), lower and higher cooling group (i.e., air
288 temperature decreased from 0°C to 2°C and from 2°C to 4°C); lower and higher rain-enhanced
289 group (i.e., precipitation increased from 0% to 20% and from 20% to 30%), lower and higher
290 rain-reduced group (i.e., precipitation decreased from 0% to 20% and from 20% to 30%). A
291 single-factor change scenario of land use was designed as the sloping upland changed into
292 forest land with the lower soil erosion rate (i.e., UFL scenario). The existing land use
293 conversion to another type, such as the change from cropland to forest land or some other land
294 use, is a kind of compromise and required a sensitivity analysis to the model simulation rather
295 than representing the conditions of the real natural system (Dey and Mishra, 2017). The IPCC's
296 Summary for Policy-makers (IPCC, 2021) points out that the average annual global land
297 precipitation is projected to increase by 10.5% and 30.2% at the $1.5\text{ }^{\circ}\text{C}$ and $4\text{ }^{\circ}\text{C}$ warming
298 levels, respectively. According to the correspondence between climate warming and increasing
299 precipitation in the IPCC's AR6, the multifactor change scenarios were designed into two
300 multiple climate change scenarios: the low and high greenhouse gas (GHG) emissions
301 scenarios. The low GHG emissions scenario represents air temperature and precipitation
302 increasing by $1.5\text{ }^{\circ}\text{C}$ and 10% , respectively, while the high one represents air temperature and

303 precipitation increasing by 4 °C and 30%, respectively. Furthermore, we also explored the
304 effect of the low and high GHG emissions scenarios in a combination of land use change
305 scenarios (i.e., UFL scenario) on sediment yield and particulate nutrient yields. The tillage
306 scenario analysis was involved in the scenario analysis of alternative management practices,
307 which were conducted as the no tillage operations in 2008. The relative change deviations of
308 the simulated annual accumulated sediment and particulate nutrient losses at the catchment
309 outlet of the designed scenarios from the baseline were provided as the quantitative evaluation
310 index for scenario analysis (Abdalla et al., 2020; Dubache et al., 2019). Moreover, the crop
311 yield changes between the designed scenarios and the baseline were evaluated in the scenario
312 analysis.

313 **2.6 Evaluation of model performance and statistical analysis**

314 The performance of the upgraded CNMM-DNDC model in simulating sediment and
315 particulate nutrient losses was evaluated using the normalized root mean square error (nRMSE),
316 the Nash–Sutcliffe index (NSI) and the slope, determination coefficient (R^2) and significance
317 level (p) of the univariate linear regression (ULR) between the simulation and observation. The
318 nRMSE and NSI values are calculated by Eq. 8 and Eq. 9, respectively. O_i and S_i are the
319 observed and simulated values, respectively. \bar{O} is the mean value of the observed data, and n
320 is the number of paired samples. If the value of nRMSE is closer to 100, the values simulated
321 by the model are more coincident with the observed values (Cui et al., 2014; Smith et al., 1997).
322 The value of the NSI provides the discrepancy between the simulated values and the mean of
323 the observed values, with a positive value indicating an acceptable simulation (Li et al., 2022a).

324 The closer to 1 the slope and R^2 of the ULR are, the better the simulated values match the
325 observed values. The Origin 8.0 (OriginLab Ltd., Guangzhou, China) and ArcGIS 10.0
326 software packages were used for graph drawing.

$$\text{nRMSE} = \frac{100}{\bar{O}} \sqrt{\frac{\sum_{i=1}^n (S_i - O_i)^2}{n}} \quad (8)$$

$$\text{NSI} = 1 - \frac{\sum_{i=1}^n (S_i - O_i)^2}{\sum_{i=1}^n (O_i - \bar{O})^2} \quad (9)$$

327 In addition, Pearson correlations were carried out to study the relationships between the
328 variables relevant to soil erosion and that related to the biogeochemistry process. The Pearson
329 correlation coefficient (r) is used to measure the correlation between two variables, with the
330 value ranging from -1 to 1 . The R project was applied for the graph drawing of the correlation
331 matrix.

332 **3. Results**

333 **3.1 Model performance in simulating soil erosion in the lysimetric plot**

334 Given the limited size of the samples, the performance of the upgraded CNMM-DNDC
335 model was revealed using only the graph of the predictions and observations (Fig. 2a–c),
336 without a quantitative evaluation with the above statistical criteria. The temporal dynamic
337 patterns of the simulated surface runoff, sediment and concomitant particulate P yields were in
338 accordance with the observed values when either model calibration or validation was
339 performed (Fig. 2 a–c). Nevertheless, on July 23, which was a heavy precipitation event (213
340 mm precipitation during the seven days prior to the observation day) in 2016, the upgraded
341 model overestimated the observed sediment yield by approximately 6 times (3.6 versus 0.6 t

342 ha^{-1} , Fig. 2b). However, the simulated surface runoff and total P loss were only approximately
343 60% and 20% larger than the observed values, respectively. Unfortunately, the simulated peaks
344 of surface runoff and sediment yield at the end of June 2015 lacked the support of the
345 observations. Moreover, we conducted an evaluation of the simulated and observed NH_4^+ and
346 NO_3^- losses accompanied by surface runoff in the lysimetric plot (Fig. S2). The upgraded
347 model generally captured the temporal variation and magnitude of the observed NH_4^+ and
348 NO_3^- loss, although discrepancies existed in the magnitude of the peak loss (i.e., the model
349 underestimated NH_4^+ loss caused by approximately 100 mm precipitation on September 4,
350 2006; Fig. S2).

351 **3.2 Model performance in simulating soil erosion at the catchment outlet**

352 The monthly observed and simulated stream flow, sediment yield, particulate and total N
353 losses at the outlet of the Jieliu catchment from 2007 to 2008 are illustrated in Fig. 3. The
354 observed stream flow and sediment yield began to increase dramatically with the concentrated
355 precipitation in summer and early autumn but rarely occurred in winter and spring (Fig. 3a–c).
356 The upgraded CNMM-DNDC model successfully predicted the above temporal pattern of the
357 stream flow and sediment yield at the catchment outlet with acceptable NSI values of 0.89 and
358 0.89 and significant ULRs with R^2 values of 0.98 and 0.96 and slope values of 0.98 and 0.90
359 for model validation, respectively (Table 1). Moreover, model validation of sediment yield
360 resulted in a larger nRMSE (38.23%) than that of stream flow simulation (34.57%).

361 The observed particulate and total N losses revealed a similar temporal pattern to that of
362 sediment yield (Fig. 3d–e) ranged from 0 to 56.3 kg mon^{-1} and 0.9 to 283.1 kg N mon^{-1} with a

363 mean value of 10.5 and 55.9 kg N mon⁻¹, respectively. The corresponding simulated particulate
364 and total N losses resulted in ranges of 0.5 to 50.4 kg N mon⁻¹ and 18.8 to 196.0 kg N mon⁻¹
365 with averages of 12.0 and 65.1 kg N mon⁻¹, respectively. The upgraded model provided an
366 overestimation of the particulate N loss in August 2007 and September 2008 by 11.3 and 14.8
367 kg N mon⁻¹, respectively. The particulate N losses in February 2007, March 2007, July 2007
368 and July 2008 and total N loss in summer were underestimated. However, in terms of the
369 validation, statistical comparisons between the simulated particulate and total N losses yielded
370 significant ULRs with R^2 values of 0.88 and 0.98 and slope values of 0.92 and 1.53, nRMSE
371 values of 57.75% and 42.55%, and NSI values of 0.74 and 0.86, respectively ($n = 12$; Table 1).
372 Meanwhile, the upgraded CNMM-DNDC model successfully predicted the temporal variation
373 and magnitudes of NO₃⁻ loss at the catchment outlet, although the model slightly
374 underestimated the peak loss in July and August of 2007 and in September of 2008 (Fig. S3).
375 The successfully prediction of the particulate N and NO₃⁻ losses and the underestimation of the
376 total N loss in July of 2007 might illustrate that the model underestimated NH₄⁺ or dissolved
377 organic N losses in July of 2007. As the above results demonstrated, the simulated and
378 observed particulate and total N losses at the catchment outlet indicated good agreement
379 despite the slight underestimation of the individual large values when heavy precipitation
380 occurred.

381 **3.3 Components of the simulated TN and PN at the catchment outlet**

382 The monthly components of TN and/or PN simulated from the original and upgraded
383 CNMM-DNDC model during the model validation of 2008 at the catchment outlet were

384 illustrated in Fig. 4. Among the TN components including PN, NH_4^+ , dissolved organic N
385 (DON) and NO_3^- , the simulation from both of the original and upgraded CNMM-DNDC
386 demonstrated that the proportion of NO_3^- at the catchment outlet was larger than that of NH_4^+
387 during the period from May to September when the larger precipitations appeared. Moreover,
388 the upgraded CNMM-DNDC demonstrated that the PN accounted for up to 16.2%–26.6% of
389 the TN components during the period with larger precipitations. Meanwhile, the labile or
390 resistant humus N accounted for 11.3%–20.3% of the PN components, though the passive
391 humus N accounted for the largest of the PN components. In addition, compared with the
392 original model, the upgraded model simulated the observed TN with smaller nRMSE (42.55%
393 versus 51.67%), better NSI (0.86 versus 0.80) and slightly improved r^2 of the ULRs (0.98
394 versus 0.97) though no significant difference was found between the original and upgraded
395 model (Fig. 4).

396 **3.4 Spatial distributions of sediment yield and particulate C, N, and P losses**

397 Figure 5 illustrated the simulated spatial distributions of the sediment yield and particulate
398 C, N, and P losses and the effects of different land uses on those in the validation year 2008.
399 The annual accumulated sediment yield simulated by the upgraded model amounted to 0–106.6
400 $\text{t ha}^{-1} \text{ yr}^{-1}$ with an average of $5.0 \text{ t ha}^{-1} \text{ yr}^{-1}$ in 2008, which was a moderate rainfall year (952
401 mm) with eight large rainstorm events (exceeding 50 mm rainfall within 24 hours). The
402 simulated annual accumulated particulate C, N, and P losses yielded 0–595.7 $\text{kg C ha}^{-1} \text{ yr}^{-1}$,
403 0–56.0 $\text{kg N ha}^{-1} \text{ yr}^{-1}$, and 0–7.9 $\text{kg P ha}^{-1} \text{ yr}^{-1}$ with averages of $63.6 \text{ kg C ha}^{-1} \text{ yr}^{-1}$, 6.1 kg N
404 $\text{ha}^{-1} \text{ yr}^{-1}$ and $0.9 \text{ kg P ha}^{-1} \text{ yr}^{-1}$, respectively. The sloping cultivated cropland areas contributed

405 to the greatest losses of sediment and particulate C, N, and P nutrients, with 68%, 60%, 58%
406 and 57% of the total, respectively. Approximately 21% of sediment loss came from the
407 residential areas as the second largest contributor to sediment loss, while the forest areas were
408 the secondary sources to particulate C, N, and P losses, with 30%, 32%, and 32% of total losses,
409 respectively. Meanwhile, the highest rates of the particulate C, N, and P losses per unit area
410 occurred in the sloping cultivated cropland areas, with 84.1 kg C ha⁻¹ yr⁻¹, 7.7 kg N ha⁻¹ yr⁻¹
411 and 1.1 kg P ha⁻¹ yr⁻¹, respectively. However, the residential areas yielded to the highest rates
412 of sediment, i.e., 8.6 t ha⁻¹ yr⁻¹. The second largest loss rates per unit area of the particulate C,
413 N, and P appeared in the residential areas. These results demonstrated that sediment yield and
414 particulate C, N, and P losses caused by surface runoff in the Jieliu catchment were directly
415 relevant to the type of land use, and the sloping cultivated cropland area became the primary
416 source of sediment yield and particulate C, N, and P losses. Meanwhile, sediment and
417 particulate C, N, and P losses from the residential areas could not be neglected.

418 Moreover, the upgraded CNMM-DNDC model coupled the biogeochemical processes
419 with soil erosion, which was able to predict the crucial variables relevant to biogeochemical
420 processes, including the productivity, greenhouse gases, contaminated gases and NO₃⁻ loss and
421 the variables related to soil erosion, including the losses of sediment and particulate C, N and P
422 (Fig. S4, Text S1).

423 **3.5 Sediment yield and particulate C, N, and P losses under different scenarios**

424 The simulated results of the single-factor change scenarios of precipitation and
425 temperature were presented in Figure 6. The sediment yield and particulate C, N, and P losses

426 (i.e., the target variables) increased with precipitation or air temperature which was reflected by
427 the positive values. The more positive the slope value is, the greater the target variables
428 increase and vice versa. The slopes between the air temperature changes of the higher and
429 lower cooling and warming scenarios and the sediment yield changes yielded -1.25 , -1.00 ,
430 -0.38 and -0.40 , respectively. Compared to the slopes of the lower warming scenarios and the
431 lower cooling scenarios, the slopes of the higher warming scenarios and the higher cooling
432 scenarios provided 21% and 5% higher yields of sediment, respectively. Meanwhile, the
433 changes in particulate C, N, and P losses provided similar but stronger responses to the higher
434 cooling scenarios. However, the particulate nutrient losses showed a complicated response to
435 the warming scenarios. The changes in the particulate nutrient losses provided an increasing
436 tendency in response to the increase of air temperature. For the lower warming scenarios, the
437 particulate nutrient losses increased with air temperature. In terms of the higher warming
438 scenarios, the particulate nutrient losses were still increasing, but the rates of increase rate
439 decreased. Compared to the baseline scenario, the scenarios with the air temperature change
440 from $0\text{ }^{\circ}\text{C}$ to $-1\text{ }^{\circ}\text{C}$ provided a slightly raising in crop yields, but the crop yields were
441 decreased as the air temperature continued to reduce. And the crop yields were reduced with
442 the increasing air temperature. These results proved that the increase in air temperature
443 decreased the losses of sediment but increased the particulate C, N, and P losses, although the
444 promoting effect became weaker for the higher warming scenarios.

445 The slopes between the precipitation changes of the higher and lower rain-reduced and
446 rain-enhanced scenarios and the sediment yield changes resulted in the values of 0.27 , 0.37 ,

447 0.52 and 0.65, respectively. In comparison with the lower rain-enhanced and rain-reduced
448 scenarios, the slopes of the higher rain-enhanced and rain-reduced scenarios provided 24%
449 higher and 34% lower yields of sediment, respectively. Meanwhile, the changes in particulate
450 nutrient losses provided similar but weaker responses to the changes in precipitation. The
451 above results demonstrated that the losses of sediment and particulate nutrients increased with
452 the increasing precipitation. In addition, the contribution from such an elevation role of
453 precipitation tended to be stronger for the higher rain-enhanced scenarios. Furthermore, the
454 changes in sediment and particulate C, N, and P losses were more sensitive to the precipitation
455 scenarios than to the temperature scenarios. The precipitation altered by the range from -30%
456 to +30% posed a minor influence on crop yields (within $\pm 0.03\%$). Comparison with the
457 baseline, the scenarios with the precipitation increasing within 18% yielded to a slightly
458 increased crop yields, while crop yields slightly decreased with the scenarios of the reducing
459 precipitation and over 20% increased precipitation.

460 Table 2 illustrated the results of the multifactor change scenarios and the land use change
461 single-factor scenario (UFL scenario). Compared to the baseline scenario, the UFL scenario
462 reduced stream flow, sediment yield, and particulate nutrient losses by -12.2%, -3.6%, -5.6%,
463 -7.0%, and -7.2%, respectively. In comparison with the baseline scenario, the low GHG
464 emissions scenario with air temperature increasing by 1.5 °C and precipitation increasing by
465 10% increased the stream flow, sediment yield and particulate C, N, and P losses by 21.2%,
466 4.1%, 5.3%, 5.3% and 5.3%, respectively. The increasing effects of the high GHG emissions
467 scenarios on the sediment and particulate nutrient losses were more than three times those of

468 the low GHG emissions scenarios. The crop yield change between the low GHG emissions
469 scenario and the baseline scenario yielded to -6.0% , while the crop yield of the high GHG
470 emissions scenario accounted for 16.6% lower than the baseline. The low GHG emissions
471 under the UFL scenario increased the stream flow and sediment yield by 5.2% and 0.2% ,
472 respectively, but decreased the particulate C, N, and P losses by -0.8% , -2.3% , and -2.5% ,
473 respectively. Moreover, the high GHG emissions under the UFL scenario increased the stream
474 flow, sediment yield, and particulate C, N, and P losses by 47.9% , 9.2% , 9.3% , 7.8% , and 7.7% ,
475 respectively. The no-tillage scenario decreased the losses of particulate nutrients by
476 approximately 2.5% , but provided almost no effect on sediment yield compared with the
477 baseline scenario (Fig. S5).

478 **3.6 Relationship among the variables relevant to soil erosion, productivity and C/N losses**

479 Figure 7 illustrated the relationships between the variables relevant to soil erosion and
480 biogeochemistry for different land use types, which were derived from model simulation. No
481 soil erosion in the winter-flooding paddy with the paddy rice-flooding fallow regime (RF)
482 because of the year-round flooding regime. For the other three land use types, the significant
483 positive correlations ($r > 0.88$) between sediment yield and particulate nutrients were found,
484 because they were entrained by water and moved with water flow. With regard to the sloping
485 uplands (SU), the particulate nutrients were significantly correlated with NO_3^- losses through
486 leaching ($r > 0.6$), though the correlation coefficient between sediment yields and NO_3^- losses
487 through leaching only yielded to 0.26 (insignificantly). For the seasonally waterlogged paddy,
488 the variables related to soil erosion (including sediment yields and particulate nutrients) were

489 negatively correlated with NH₃ emissions ($r > 0.65$), while they were positively correlated with
490 NO₃⁻ losses through runoff ($r < -0.61$). As to the forest land (FL), significantly positive
491 correlations between the variables related to soil erosion and NO₃⁻ losses through
492 leaching/runoff were found ($r > 0.72$), which might be because all these variables were related
493 to the precipitation. The productivity performed negative impacts on sediment yield and
494 particulate nutrients in the RF an FL systems while the productivity provided a slightly
495 negative impact on sediment yield but a slightly positive impact on the particulate nutrients in
496 the SP system.

497 **4. Discussion**

498 **4.1 Effect of land use on soil erosion and particulate C, N, and P losses**

499 Land use change has been considered one of the most important factors affecting the
500 intensity and distribution of surface runoff and soil erosion (Dunjó et al., 2004; Kosmas et al.,
501 1997; Wei et al., 2007; Zhang et al., 2021b). Our study also provided consistent results, which
502 indicated that the intensity of soil erosion and the corresponding particulate C, N, and P losses
503 in the Jieliu catchment were closely related to land use, with the following order: sloping
504 cultivated cropland > residential area > forest land. The residential area with the waterproofed
505 concrete roads and residential buildings, which was the secondary source to soil erosion, might
506 be because it provided the largest surface runoff among these three land use types in the
507 concerned year of 2008 (Fig. S6), though the limited soil was exposed for erosion. There were
508 three major reasons why forest land contributed to the lowest losses of sediment and particulate
509 nutrients among the above three land uses. First, canopy interception reduced the amount of
510 rainfall reaching the ground, which directly decreased the occurrence of runoff and associated

511 erosion (Greene and Hairsine, 2004; Hou et al., 2020; Vasquez-Mendez et al., 2010). Several
512 previous studies also reported that forest land with a thick canopy exhibited a lower amount of
513 runoff than did other land uses (Mehri et al., 2018; Mohammad and Adam, 2010; Nunes et al.,
514 2011). Fortunately, the direct protection mechanism by canopy interception was involved in
515 the CNMM-DNDC model, which was calculated using the leaf area index (Zhang et al., 2018).
516 Second, the litter cover of forest land protects the soil surface from the direct splash and
517 detachment of raindrops, which can decrease the formation of mechanical crusts and increase
518 the infiltration capacity and hence diminish the potential for surface runoff and soil erosion
519 (Casermeiro et al., 2004; Lemenih et al., 2005; Wainwright et al., 2002). However, the
520 CNMM-DNDC did not take the protection of litter cover on the soil surface into consideration.
521 Further observation data and studies are needed to introduce the mechanism of the effect of
522 litter cover on surface runoff and soil sediment into the CNMM-DNDC model. Last, forest
523 land is equipped with higher soil organic matter and hydraulic conductivity than other land
524 uses, which can indirectly enhance soil infiltration and reduce surface runoff (Abrishamkesh et
525 al., 2011; Fu et al., 2000; Lemenih et al., 2004). The excellent soil properties of forest land soil
526 (e.g., higher soil organic matter and vertical saturated hydraulic conductivity) have been
527 involved in the CNMM-DNDC model inputs. Moreover, as the forest litterfall returned to the
528 soil and participated in further C and N cycling, the content of soil organic matter was
529 enhanced and accumulated. With regard to the scenario analysis, we found that the scenarios
530 related to the forest land contributed to greater decreases in sediment yield than surface runoff
531 (Table 2). The results of the lysimetric plot experiments by Chen et al. (2012) also

532 demonstrated that vegetation types and human interference had a relatively small impact on
533 surface runoff but had an appreciable effect on sediment yield.

534 The canopy of the cultivated cropland served as a weaker hindrance to rainfall, which
535 suffered from more surface runoff, than that of the forest canopy. However, the different
536 effects on soil erosion and rainfall interception by various crop planting density (Panagos et al.,
537 2015a), e.g., the wide row maize and the dense grass-like wheat, and different crop types
538 (Williamm, 1990) needed more observations to modify and evaluate the CNMM-DNDC in
539 future. Furthermore, frequent agricultural activities (i.e., tillage) loosen the subsurface soil and
540 nutrients, which raises the risk of soil erosion and the associated loss of particulate nutrients
541 (Gregorich et al., 1998; Moldenhauer et al., 1967; Muukkonen et al., 2009). The
542 CNMM-DNDC model has taken the vertical mixing effect of tillage on the chemical soil
543 properties into consideration, and this process left the subsurface soil organic nutrients
544 unprotected and prone to erosion. This explained the reduction in particulate C, N, and P
545 nutrient losses under the no-tillage scenarios (Fig. S5). However, several studies found that
546 tillage disturbed the soil structure and pore size distribution (Carof et al., 2007; Castellini and
547 Ventrella, 2012; Kay and VandenBygaart, 2002; Nunes et al., 2010), which made the effect of
548 agricultural activities on surface runoff and soil erosion difficult to model (Leitinger et al.,
549 2010). Given that the vertical mixing effect of tillage on soil chemical properties instead of soil
550 physical properties was considered in the CNMM-DNDC, the yields of surface runoff and
551 sediment resulting from the no-tillage scenario were not decreased compared with the baseline
552 scenario with tillage (Fig. S5).

553 4.2 Effect of climate change on soil erosion and particulate C, N, and P losses

554 In past decades, the frequent occurrence of warming and extreme weather events (e.g.,
555 extreme precipitation events) has been irrefutable (IPCC, 2019). From 1998 to 2021, the
556 observed annual average air temperature and annual precipitation in the Jieliu catchment also
557 presented an increasing trend but did not have a significant regression relationship (Fig. S7). In
558 CNMM-DNDC, the biogeochemical processes were strongly influenced by air or soil
559 temperature (Table S4). There were two reasons why the simulated soil erosion responded to
560 the air temperature changes. On one hand, the vegetation growth was sensitive to the air
561 temperature changes, which affected the C_v which was the effect factor of the soil erosion in Eq.
562 1. The increasing air temperature provided a positive effect on the vegetation growth (e.g., leaf
563 area index, Fig. S8), which increased the precipitation interception by canopy to direct decrease
564 the soil erosion. However, the raising air temperature might shorten the duration of the
565 vegetation growth period, which directly shortened the period of the soils protected by crop
566 canopy and lengthened the time of the bare soils exposed to the surface runoff increasing the
567 risk of erosion (Fig. S8). This increasing risk of sediment yield when air temperature increased
568 was not shown in this case might because that the heavy rainfall events almost occurred the
569 duration with vegetation growth (Fig. S8). Besides, the decreasing air temperature weakened
570 the processes of the respiration and photosynthesis, which led to a slower vegetation growth
571 (Fig. S8). On the other hand, compared to the baseline scenarios, the climate warming
572 scenarios, with a better vegetation growth, conducted a higher evapotranspiration, which led to
573 a reduction on soil moisture content, to indirectly reduce the surface runoff and soil erosion.

574 The asymmetric response of sediment yield and particulate nutrient losses to the cooling and
575 warming scenarios might result from the different effects of the cooling and warming of air
576 temperature on the vegetation growth. The growth of vegetation was strongly inhibited by the
577 low temperature in the cooling scenarios through affecting the duration and start time of the
578 phenological stages. Our results of the scenario analysis indicated that the losses of sediment
579 slightly decreased with the scenarios treated with climate warming alone, which lay in the
580 higher C_v caused by the enhanced vegetation growth (Ficklin et al., 2009; Zhang et al., 2020a;
581 Zhou et al., 2003). We found that the decreasing effect of increasing air temperature on
582 sediment loss decreased (especially for the scenario with an air temperature increase of 4 °C,
583 Fig. 6), which might be because the enhanced effect of increasing air temperature on vegetation
584 growth is not unlimited. Once the air temperature exceeds the threshold of the optimum
585 temperature for photosynthesis and vegetation growth, it would have a negative or even
586 harmful impact on plant growth (Chapin, 1983; Schlenker and Roberts, 2009). The complex
587 response of the particulate C, N, and P losses to air temperature increased, probably because
588 they increased with the enrichment ratio and sediment yield, but the enrichment ratio decreased
589 with sediment. Therefore, the slightly increasing sediment with increasing air temperature and
590 the corresponding decreasing enrichment ratio might lead to upward or downward fluctuations
591 in particulate C, N, and P losses. However, we found that the rate of soil loss increased with
592 increasing precipitation amount and the corresponding increase in heavy rain events. Jiang et al.
593 (2017) also found that the increase in sediment loss was amplified by the increased
594 precipitation, which was directly accompanied by a dramatic and sustained increase in surface

595 runoff. Therefore, the higher GHG emissions scenarios, in which the soil erosion provided a
596 higher increase response to the rising precipitation and a lower and smaller decrease response
597 to the rising air temperature, might provide a greater risk of soil erosion than the low GHG
598 emissions scenario. Overall, our results indicated that the hydrology of the Jieliu catchment is
599 very sensitive to potential future climate changes, especially to the higher GHG emissions
600 scenarios.

601 **4.3 Interactive effect of climate and land use change on soil and nutrient losses**

602 Changes in either climate or land use imply considerable influences on water and nutrient
603 cycles in a catchment or region (Labat et al., 2004; Milliman et al., 2008; Piao et al., 2007; Yin
604 et al., 2017). Our simulated results indicated that the reduction extent of the UFL scenario on
605 soil erosion, especially on sediment yield and associated nutrient losses, offset the increasing
606 extent caused by the low GHG emissions scenario. However, the UFL scenario was insufficient
607 to totally offset the sediment and particulate C, N, and P losses caused by the high GHG
608 emissions scenario. Nevertheless, vegetation restoration might still be able to slow the soaring
609 process of soil erosion caused by climate change in the future. Previous studies primarily
610 focused on the effects of human activity and climate change on the changes in surface runoff or
611 stream flow. Wang et al. (2016) demonstrated that human activity contributed to slightly larger
612 effects on stream flow changes than climate (59% versus 41%) by analyzing the long-term
613 records of hydrological data in the Luan River basin in North China. The results in the Heihe
614 River basin in Northwest China showed that human activities were the dominant contributor to
615 the variation in runoff in the upper and middle reaches when compared to climate change (Qiu

616 et al., 2015). However, other studies have shown that the influence of climate change on soil
617 and water loss was greater than that of human activities. Jiang et al. (2017) pointed out that
618 climate change, in comparison with anthropogenic activities, was the primary factor causing
619 the changes in either stream flow or sediment discharge in the Yellow River basin and Yangtze
620 River basin in China. The Huron River catchment in southeastern Michigan in the U.S.A. was
621 more sensitive to climate change than to land use change, as demonstrated by Barlage et al.
622 (2002).

623 Furthermore, we found that the promoting impacts of both high and low GHG emissions
624 scenarios on surface runoff were greater than those on sediment yield and associated
625 particulate nutrient losses. In contrast, the reduction effect of the UFL scenarios on sediment
626 yield and associated particulate nutrient losses was stronger than that on surface runoff (Table
627 2). These results demonstrated that human activity, e.g., the conversion from cropland with
628 intensive human disturbance to forest land, resulted in a greater mitigation effect on sediment
629 yield and associated particulate nutrient losses than on surface runoff. Therefore, further
630 studies should consider the effects of human activity and climate change on surface runoff and
631 on soil erosion as well as the associated nutrient losses. In summary, reasonable human
632 intervention, such as rational land use change, is expected to be a feasible practice to decelerate
633 soil erosion and associated particulate nutrient losses without altering and disturbing the
634 hydrological cycle of a catchment in the context of global warming.

635 **Conclusions**

636 The hydro-biogeochemical model (CNMM-DNDC) was improved by introducing the soil

637 erosion physical model (adopted from the simplified ROSE model) and the element (i.e.,
638 carbon, nitrogen and phosphorus) enrichment module to estimate soil erosion and the
639 movements of particulate nutrients. The comparability between the simulation and observation,
640 including surface runoff, sediment yield, and particulate nitrogen and phosphorus losses at the
641 lysimetric plot and the stream flow, sediment yield, and particulate N loss at the outlet of Jieliu
642 catchment, demonstrated that the upgraded CNMM-DNDC model could reliably simulate soil
643 erosion and the consequential particulate nutrient losses. The spatial distribution characteristics
644 of sediment yield and the consequential particulate carbon, nitrogen and phosphorus losses
645 were directly related to the spatial distribution of land use type, among which the sloping
646 cultivated cropland areas contributed to the greatest losses. The analysis of climate
647 single-factor change scenarios implied that the high GHG emissions scenarios provided a
648 greater potential risk of soil erosion, which resulted in the larger soil erosion rates than those in
649 the low GHG emissions scenarios. The scenarios with all non-forest land changes into forest
650 land decreased stream flow, sediment yield and particulate C, N, and P losses compared to the
651 baseline scenario. Anthropogenic activities (e.g., land use change) might be expected to help
652 mitigate the processes of soil and water losses accelerated by climate change in the future.

653 **Code and data availability**

654 The CNMM-DNDC model was originally developed by the Institute of Atmospheric
655 Physics using C++ language, which can be run on a standard PC. The upgraded model is
656 available on the FigShare (<https://doi.org/10.6084/m9.figshare.20210546>).

657 **Author contribution**

658 Siqi Li arranged data, improved model and implemented the simulation, prepared the

659 original draft. Yong Li, Xunhua Zheng, Wei Zhang developed the conceptualization and
660 methodology of this study. Bo Zhu, Pengcheng Hu, Jihui Fan, Tao Wang collected and
661 arranged data. Shenghui Han, Rui Wang, Kai Wang analyzed data and verified the results.
662 Zhisheng Yao, Chunyan Liu improved the conceptualization and writing.

663 **Acknowledgments**

664 This work was supported by the Chinese Academy of Sciences (grant number:
665 ZDBS-LY-DQC007; XDA23070100), the National Key R&D Program of China (grant number:
666 2022YFE0209200), the special fund of State Environmental Protection Key Laboratory of
667 Formation and Prevention of Urban Air Pollution Complex (grant number:
668 SEPAir-2022080590), the National Key Scientific and Technological Infrastructure project
669 “Earth System Science Numerical Simulator Facility” (EarthLab), the National Natural Science
670 Foundation of China (grant number: 41907280, U22A20562), and the China Postdoctoral
671 Science Foundation (grant number: 2019M650808).

672 **Competing interests**

673 The authors declare that they have no conflict of interest.

674 **References**

675 Abdalla, M., Song, X., Ju, X., Topp, C., and Smith, P.: Calibration and validation of the
676 DNDC model to estimate nitrous oxide emissions and crop productivity for a summer
677 maize-winter wheat double cropping system in Hebei, China, *Environmental Pollution*, 262,
678 114199, <https://doi.org/10.1016/j.envpol.2020.114199>, 2020.

679 Abrishamkesh, S., Gorji, M., and Asadi, H.: Long-term effects of land use on soil
680 aggregate stability, *International Agrophysics*, 25, 103–108,

681 <http://www.international-agrophysics.org/Long-term-effects-of-land-use-on-soil-aggregate-stab>
682 [ility,106297,0,2.html](http://www.international-agrophysics.org/Long-term-effects-of-land-use-on-soil-aggregate-stability,106297,0,2.html), 2011.

683 Arnold, J., Srinivasan, R., Muttiah, R., and Williams, J.: Large area hydrologic modeling
684 and assessment part I: model development, *Journal of the American Water Resources*
685 *Association*, 34, 73–89, <https://doi.org/10.1111/j.1752-1688.1998.tb05961.x>, 1998.

686 Barlage, M., Richards, P., Sousounis, P., and Brenner, A.: Impacts of climate change and
687 land use change on runoff from a Great Lakes watershed, *Journal of Great Lakes Research*, 28,
688 568–582, [https://doi.org/10.1016/S0380-1330\(02\)70606-0](https://doi.org/10.1016/S0380-1330(02)70606-0), 2002.

689 Berhe, A., Barnes, R., Six, J., and Marín-Spiotta, E.: Role of Soil Erosion in
690 Biogeochemical Cycling of Essential Elements: Carbon, Nitrogen, and Phosphorus, *Annual*
691 *Review of Earth and Planetary Sciences*, 46, 521–548,
692 <https://doi.org/10.1146/annurev-earth-082517-010018>, 2018.

693 Carof, M., De Tourdonnet, S., Coquet, Y., Hallaire, V., and Roger-Estrade, J.: Hydraulic
694 conductivity and porosity under conventional and no-tillage and the effect of three species of
695 cover crop in northern France, *Soil Use and Management*, 23, 230–237,
696 <https://doi.org/10.1111/j.1475-2743.2007.00085.x>, 2007.

697 Casermeiro, M., Molina, J., Caravaca, M., Costa, J., Massanet, M., and Moreno, P.:
698 Influence of scrubs on runoff and sediment loss in soils of Mediterranean climate, *Catena*, 57,
699 91–107, [https://doi.org/10.1016/s0341-8162\(03\)00160-7](https://doi.org/10.1016/s0341-8162(03)00160-7), 2004.

700 Castellini, M. and Ventrella, D.: Impact of conventional and minimum tillage on soil
701 hydraulic conductivity in typical cropping system in Southern Italy, *Soil and Tillage Research*,

702 124, 47–56, <https://doi.org/10.1016/j.still.2012.04.008>, 2012.

703 Chapin, F.: Direct and indirect effects of temperature on arctic plants, *Polar Biology*, 2,
704 47–52, <https://doi.org/10.1007/BF00258285>, 1983.

705 Chen, H., Yang, J., Fu, W., He, F., and Wang, K.: Characteristics of slope runoff and
706 sediment yield on karst hill-slope with different land-use types in northwest Guangxi,
707 *Transactions of the Chinese Society of Agricultural Engineering*, 28, 121–126,
708 <https://doi.org/10.3969/j.issn.1002-6819.2012.16.019>, 2012.

709 Cui, F., Zheng, X., Liu, C., Wang, K., Zhou, Z., and Deng, J.: Assessing biogeochemical
710 effects and best management practice for a wheat-maize cropping system using the DNDC
711 model, *Biogeosciences*, 11, 91–107, <https://doi.org/10.5194/bg-11-91-2014>, 2014.

712 Deng, J., Zhou, Z., Zhu, B., Zheng, X., Li, C., Wang, X., and Jian, Z.: Modeling nitrogen
713 loading in a small watershed in southwest China using a DNDC model with hydrological
714 enhancements, *Biogeosciences*, 8, 2999–3009, <https://doi.org/10.5194/bg-8-2999-2011>, 2011.

715 Dey, P. and Mishra, A.: Separating the impacts of climate change and human activities on
716 streamflow: a review of methodologies and critical assumptions, *Journal of Hydrology*, 548,
717 278–290, <https://doi.org/10.1016/j.jhydrol.2017.03.014>, 2017.

718 Donovan, M.: Modelling soil loss from surface erosion at high-resolution to better
719 understand sources and drivers across land uses and catchments; a national-scale assessment of
720 Aotearoa, New Zealand, *Environmental Modelling & Software*, 147, 105228,
721 <https://doi.org/10.1016/j.envsoft.2021.105228>, 2022.

722 Dubache, G., Li, S., Zheng, X., Zhang, W., and Deng, J.: Modeling ammonia

723 volatilization following urea application to winter cereal fields in the United Kingdom by a
724 revised biogeochemical model, *Science of The Total Environment*, 660, 1403–1418,
725 <https://doi.org/10.1016/j.scitotenv.2018.12.407>, 2019.

726 Dunjó, G., Pardini, G., and Gispert, M.: The role of land use–land cover on runoff
727 generation and sediment yield at a microplot scale, in a small Mediterranean catchment,
728 *Journal of Arid Environments*, 57, 99–116, [https://doi.org/10.1016/S0140-1963\(03\)00097-1](https://doi.org/10.1016/S0140-1963(03)00097-1),
729 2004.

730 Ekholm, P. and Lehtoranta, J.: Does control of soil erosion inhibit aquatic eutrophication,
731 *Journal of Environmental Management*, 93, 140–146,
732 <https://doi.org/10.1016/j.jenvman.2011.09.010>, 2012.

733 Ferrant, S., Oehler, F., Durand, P., Ruiz, L., Salmon-Monviola, J., Justes, E., Dugast, P.,
734 Probst, A., Probst, J., and Sanchez-Perez, J.: Understanding nitrogen transfer dynamics in a
735 small agricultural catchment: comparison of a distributed (TNT2) and a semi distributed
736 (SWAT) modeling approaches, *Journal of Hydrology*, 406, 1–15,
737 <https://doi.org/10.1016/j.jhydrol.2011.05.026>, 2011.

738 Ficklin, D., Luo, Y., Luedeling, E., and Zhang, M.: Climate change sensitivity assessment
739 of a highly agricultural watershed using SWAT, *Journal of Hydrology*, 374, 16–29,
740 <https://doi.org/10.1016/j.jhydrol.2009.05.016>, 2009.

741 Fu, B., Chen, L., Ma, K., Zhou, H., and Wang, J.: The relationships between land use and
742 soil conditions in the hilly area of the loess plateau in northern Shaanxi, China, *Catena*, 39,
743 69–78, [https://doi.org/10.1016/s0341-8162\(99\)00084-3](https://doi.org/10.1016/s0341-8162(99)00084-3), 2000.

744 Garcia-Ruiz, J., Begueria, S., Nadal-Romero, E., Gonzalez-Hidalgo, J., Lana-Renault, N.,
745 and Sanjuan, Y.: A meta-analysis of soil erosion rates across the world, *Geomorphology*, 239,
746 160–173, <https://doi.org/10.1016/j.geomorph.2015.03.008>, 2015.

747 Greene, R. and Hairsine, P.: Elementary processes of soil-water interaction and thresholds
748 in soil surface dynamics: a review, *Earth Surface Processes and Landforms*, 29, 1077–1091,
749 <https://doi.org/10.1002/esp.1103>, 2004.

750 Gregorich, E., Greer, K., Anderson, D., and Liang, B.: Carbon distribution and losses:
751 erosion and deposition effects, *Soil and Tillage Research*, 47, 291–302,
752 [https://doi.org/10.1016/S0167-1987\(98\)00117-2](https://doi.org/10.1016/S0167-1987(98)00117-2), 1998.

753 Hou, G., Bi, H., Huo, Y., Wei, X., Zhu, Y., Wang, X., and Liao, W.: Determining the
754 optimal vegetation coverage for controlling soil erosion in *Cynodon dactylon* grassland in
755 North China, *Journal of Cleaner Production*, 244, 118771,
756 <https://doi.org/10.1016/j.jclepro.2019.118771>, 2020.

757 Hu, P.: Applicability of revised DNDC model to simulate phosphorus migration on the
758 slope farmland of purple soil, Institute of Mountain Hazards and Environment, University of
759 Chinese Academy of Sciences, Chengdu, 2020.

760 IPCC: Climate Change and Land: an IPCC Special Report on Climate Change,
761 Desertification, Land Degradation, Sustainable Land Management, Food Security, and
762 Greenhouse Gas Fluxes in Terrestrial Ecosystems, 2019.

763 IPCC: Sixth Assessment Report: Working Group I: Summary for Policemakers, 2021.

764 Jetten, V., Govers, G., and Hessel, R.: Erosion models: quality of spatial predictions,

765 Hydrological Processes, 17, 887–900, <https://doi.org/10.1002/hyp.1168>, 2003.

766 Jiang, C., Zhang, L., and Tang, Z.: Multi-temporal scale changes of streamflow and
767 sediment discharge in the headwaters of Yellow River and Yangtze River on the Tibetan
768 Plateau, China, Ecological Engineering, 102, 240–254,
769 <https://doi.org/10.1016/j.ecoleng.2017.01.029>, 2017.

770 Kay, B. and VandenBygaart, A. : Conservation tillage and depth stratification of porosity
771 and soil organic matter, Soil and Tillage Research, 66, 107–118,
772 [https://doi.org/10.1016/S0167-1987\(02\)00019-3](https://doi.org/10.1016/S0167-1987(02)00019-3), 2002.

773 Kosmas, C., Danalatos, N., Cammeraat, L., Chabart, M., Diamantopoulos, J., Farand, R.,
774 Gutierrez, L., Jacob, A., Marques, H., Martinez-Fernandez, J., Mizara, A., Moustakas, N.,
775 Nicolau, J., Oliveros, C., Pinna, G., Puddu, R., Puigdefabregas, J., Roxo, M., Simao, A.,
776 Stamou, G., Tomasi, N., Usai, D., and Vacca, A.: The effect of land use on runoff and soil
777 erosion rates under Mediterranean conditions, Catena, 29, 45–59,
778 [https://doi.org/10.1016/S0341-8162\(96\)00062-8](https://doi.org/10.1016/S0341-8162(96)00062-8), 1997.

779 Labat, D., Godderis, Y., Probst, J., and Guyot, J.: Evidence for global runoff increase
780 related to climate warming, Advances in Water Resources, 27, 631–642,
781 <https://doi.org/10.1016/j.advwatres.2004.02.020> ,2004.

782 Leitinger, G., Tasser, E., Newesely, C., Obojes, N., and Tappeiner, U.: Seasonal dynamics
783 of surface runoff in mountain grassland ecosystems differing in land use, Journal of Hydrology,
784 385, 95–104, <https://doi.org/10.1016/j.jhydrol.2010.02.006>, 2010.

785 Lemenih, M., Karlton, E., and Olsson, M.: Assessing soil chemical and physical property

786 responses to deforestation and subsequent cultivation in smallholders farming system in
787 Ethiopia, *Agriculture, Ecosystems & Environment*, 105, 373–386,
788 <https://doi.org/10.1016/j.agee.2004.01.046>, 2005.

789 Lemenih, M., Olsson, M., and Karlton, E.: Comparison of soil attributes under *Cupressus*
790 *lusitanica* and *Eucalyptus saligna* established on abandoned farmlands with continuously
791 cropped farmlands and natural forest in Ethiopia, *Forest Ecology and Management*, 195, 57–67,
792 <https://doi.org/10.1016/j.foreco.2004.02.055>, 2004.

793 Li, C., Frohling, S., and Frohling, T.: A model of nitrous oxide evolution from soil driven
794 by rainfall events: 1. Model structure and sensitivity, *Journal of Geophysical*
795 *Research–Atmospheres*, 97, 9759–9776, <https://doi.org/10.1029/92jd00509>, 1992.

796 Li, S., Li, Y., Zhang, W., Zheng, X., Hu, P., Fan, J., Wang, T., and Zhu, B.: Simulation of
797 water-induced erosion and transport of particulate elements in catchment by extending the
798 CNMM-DNDC model, *Chinese Journal of Eco-Agriculture*, 30(9), 1511–1521,
799 <https://doi.org/10.12357/cjea.20210781>, 2022a.

800 Li, S., Zhang, W., Zheng, X., Li, Y., Han, S., Wang, R., Wang, K., Yao, Z., Liu, C., and
801 Zhang, C.: Update a biogeochemical model with process-based algorithms to predict ammonia
802 volatilization from fertilized uplands and rice paddy fields, *Biogeosciences*, 2022, 3001–3019,
803 <https://doi.org/10.5194/bg-19-3001-2022>, 2022b.

804 Li, Y., Shen, J., Wang, Y., Gao, M., Liu, F., and Zhou, P.: CNMM: a grid-based
805 spatially-distributed catchment simulation model, China Science Press, Beijing, 2017.

806 Liu, Y., Fu, B., Liu, Y., Zhao, W., and Wang, S.: Vulnerability assessment of the global

807 water erosion tendency: vegetation greening can partly offset increasing rainfall stress, *Land*
808 *Degradation & Development*, 30, 1061–1069, <https://doi.org/10.1002/ldr.3293>, 2019.

809 Loch, R. and Donnollan, T.: Field rainfall simulator studies on two clay soils of the
810 Darling Downs, Queensland. II. Aggregate breakdown, sediment properties and soil erodibility,
811 *Australian Journal of Soil Research*, 21, 47–58, <https://doi.org/10.1071/sr9830047>, 1983.

812 Ma, X., Zhao, C., and Zhu, J.: Aggravated risk of soil erosion with global warming: a
813 global meta-analysis, *Catena*, 200, 105129, <https://doi.org/10.1016/j.catena.2020.105129>,
814 2021.

815 Massey, H. and Jackson, M.: Selective erosion of soil fertility constituents, *Soil Science*
816 *Society of America Proceedings*, 16, 353–356,
817 <https://doi.org/10.2136/sssaj1952.03615995001600040008x>, 1952.

818 McElroy, A., Chiu, S., Nebgen, J., and Bennett, F.: Loading functions for assessment of
819 water pollution from nonpoint sources, Midwest Research Institute, Kansas City, 1976.

820 Mehri, A., Salmanmahiny, A., Tabrizi, A., Mirkarimi, S., and Sadoddin, A.: Investigation
821 of likely effects of land use planning on reduction of soil erosion rate in river basins: case study
822 of the Gharesoo River Basin, *Catena*, 167, 116–129,
823 <https://doi.org/10.1016/j.catena.2018.04.026>, 2018.

824 Meinen, B. and Robinson, D.: From hillslopes to watersheds: Variability in model
825 outcomes with the USLE, *Environmental Modelling & Software*, 146, 105229,
826 <https://doi.org/10.1016/j.envsoft.2021.105229>, 2021.

827 Milliman, J., Farnsworth, K., Jones, P., Xu, K., and Smith, L.: Climatic and anthropogenic

828 factors affecting river discharge to the global ocean, 1951–2000, *Global and Planetary Change*,
829 62, 187–194, <https://doi.org/10.1016/j.gloplacha.2008.03.001>, 2008.

830 Mohammad, A. and Adam, M.: The impact of vegetative cover type on runoff and soil
831 erosion under different land uses, *Catena*, 81, 97–103,
832 <https://doi.org/10.1016/j.catena.2010.01.008>, 2010.

833 Moldenhauer, W., Wischmei, W., and Parker, D.: Influence of crop management on runoff
834 erosion and soil properties of a Marshall silty clay loam, *Soil Science Society of America*
835 *Proceedings*, 31, 541–546, <https://doi.org/10.2136/sssaj1967.03615995003100040031x>, 1967.

836 Muukkonen, P., Hartikainen, H., and Alakukku, L.: Effect of soil structure disturbance on
837 erosion and phosphorus losses from Finnish clay soil, *Soil and Tillage Research*, 103, 84–91,
838 <https://doi.org/10.1016/j.still.2008.09.007>, 2009.

839 Nunes, A., de Almeida, A., and Coelho, C.: Impacts of land use and cover type on runoff
840 and soil erosion in a marginal area of Portugal, *Applied Geography*, 31, 687–699,
841 <https://doi.org/10.1016/j.apgeog.2010.12.006>, 2011.

842 Nunes, A., Coelho, C., de Almeida, A., and Figueiredo, A.: Soil erosion and hydrological
843 response to land abandonment in a central inland area of Portugal, *Land Degradation &*
844 *Development*, 21, 260–273, <https://doi.org/10.1002/ldr.973>, 2010.

845 Panagos P., Borrelli P., Meusburger K., Alewell C.: Lugato E., Montanarella L.:
846 Estimating the soil erosion cover-management factor at the European scale, *Land Use Policy*,
847 48, 38–50, <https://doi.org/10.1016/j.landusepol.2015.05.012>, 2015a.

848 Panagos P., Borrelli P., Meusburger K., Zanden E., Poesen J., Alewell C.: Modelling the

849 effect of support practices (P-factor) on the reduction of soil erosion by water at European
850 scale. *Environmental science & policy*, 51, 23–34,
851 <http://dx.doi.org/10.1016/j.envsci.2015.03.012>, 2015b.

852 Panagos, P., Borrelli, P., and Robinson, D.: Tackling soil loss across Europe, *Nature*, 526,
853 195, <https://doi.org/10.1038/526195d>, 2015c. Piao, S., Friedlingstein, P., Ciais, P., de
854 Noblet-Ducoudré, N., Labat, D., and Zaehle, S.: Changes in climate and land use have a larger
855 direct impact than rising CO₂ on global river runoff trends, *Proceedings of the National*
856 *Academy of Sciences of the United States of America*, 104, 15242–15247,
857 <https://doi.org/10.1073/pnas.0707213104>, 2007.

858 Pohlert, T., Huisman, J., Breuer, L., and Frede, H.: Integration of a detailed
859 biogeochemical model into SWAT for improved nitrogen predictions: model development,
860 sensitivity, and GLUE analysis, *Ecological Modelling*, 203, 215–228,
861 <https://doi.org/10.1016/j.ecolmodel.2006.11.019>, 2007.

862 Qiu, L., Peng, D., Xu, Z., and Liu, W.: Identification of the impacts of climate changes
863 and human activities on runoff in the upper and middle reaches of the Heihe River basin, China,
864 *Journal of Water and Climate Change*, 7, 251–262, <https://doi.org/10.2166/wcc.2015.115>,
865 2015.

866 Renard, K., Foster, G., Weesies, G., McCool, D., and Yoder, D.: Predicting soil erosion by
867 water: a guide to conservation planning with the Revised Universal Soil Loss equation
868 (RUSLE), Agricultural Handbook Service, United States Department of Agriculture,
869 Washington, 1997.

870 Rose, C., Williams, J., Sander, G., and Barry, D.: A mathematical model of soil erosion
871 and deposition processes: I. theory for a plane land element, *Soil Science Society of America*
872 *Journal*, 47, 991–995, <https://doi.org/10.2136/sssaj1983.03615995004700050030x>, 1983.

873 Schiettecatte, W., Gabriels, D., Cornelis, W., and Hofman, G.: Enrichment of organic
874 carbon in sediment transport by interrill and rill erosion processes, *Soil Science Society of*
875 *America Journal*, 72, 50–55, <https://doi.org/10.2136/sssaj2007.0201>, 2008.

876 Schlenker, W. and Roberts, M.: Nonlinear temperature effects indicate severe damages to
877 US crop yields under climate change, *Proceedings of the National Academy of Sciences of the*
878 *United States of America*, 106, 15594–15598, <https://doi.org/10.1073/pnas.0906865106>, 2009.

879 Sharpley, A.: The enrichment of soil Phosphorus in runoff sediments, *Journal of*
880 *Environmental Quality*, 9, 521–526, <https://doi.org/10.2134/jeq1980.00472425000900030039x>,
881 1980.

882 Smith, P., Smith, J., Powlson, D., McGill, W., Arah, J., Chertov, O., Coleman, K., Franko,
883 U., Frolking, S., Jenkinson, D., Jensen, L., Kelly, R., Klein-Gunnewiek, H., Komarov, A., Li,
884 C., Molina, J., Mueller, T., Parton, W., Thornley, J., and Whitmore, A.: A comparison of the
885 performance of nine soil organic matter models using datasets from seven long-term
886 experiments, *Geoderma*, 81, 153–225, [https://doi.org/10.1016/s0016-7061\(97\)00087-6](https://doi.org/10.1016/s0016-7061(97)00087-6), 1997.

887 Stewart, B.: *Advance in soil science*, Springer-Verlag, New York Berlin Heidelberg Tokyo,
888 18–55, 1985.

889 Sumner, H., Wauchope, R., Truman, C., Dowler, C., and Hook, J.: Rainfall simulator and
890 plot design for mesoplot runoff studies, *Transactions of the ASAE*, 39, 125–130,

891 <https://doi.org/10.13031/2013.27489>, 1996.

892 Teixeira, P. and Misra, R.: Measurement and prediction of nitrogen loss by simulated
893 erosion events on cultivated forest soils of contrasting structure, *Soil and Tillage Research*, 83,
894 204–217, <https://doi.org/10.1016/j.still.2004.07.014>, 2005.

895 Vasquez-Mendez, R., Ventura-Ramos, E., Oleschko, K., Hernandez-Sandoval, L., Parrot,
896 J., and Nearing, M.: Soil erosion and runoff in different vegetation patches from semiarid
897 Central Mexico, *Catena*, 80, 162–169, <https://doi.org/10.1016/j.catena.2009.11.003>, 2010.

898 Wainwright, J., Parsons, A., Schlesinger, W., and Abrahams, A.: Hydrology–vegetation
899 interactions in areas of discontinuous flow on a semi-arid bajada, Southern New Mexico,
900 *Journal of Arid Environments*, 51, 319–338, <https://doi.org/10.1006/jare.2002.0970>, 2002.

901 Wan, Y. and El-Swaify, S.: Sediment enrichment mechanisms of organic carbon and
902 phosphorus in a well-aggregated Oxisol, *Journal of Environmental Quality*, 27, 132–138,
903 <https://doi.org/10.2134/jeq1998.00472425002700010019x>, 1998.

904 Wang, H., Chen, L., and Yu, X.: Distinguishing human and climate influences on
905 streamflow changes in Luan River basin in China, *Catena*, 136, 182–188,
906 <https://doi.org/10.1016/j.catena.2015.02.013>, 2016.

907 Wei, W., Chen, L., Fu, B., Huang, Z., Wu, D., and Gui, L.: The effect of land uses and
908 rainfall regimes on runoff and soil erosion in the semi-arid loess hilly area, China, *Journal of*
909 *Hydrology*, 335, 247–258, <https://doi.org/10.1016/j.jhydrol.2006.11.016>, 2007.

910 William J.: The erosion-productivity impact calculator (EPIC) model: a case history,
911 *Philosophical Transactions of the Royal Society*, 329, 421–428,

912 <https://doi.org/10.1098/rstb.1990.0184>, 1990.

913 Williams, J.: Sediment routing for agricultural watersheds, Journal of the American Water
914 Resources Association, 11, 965–974, <https://doi.org/10.1111/j.1752-1688.1975.tb01817.x>,
915 1975.

916 Williams, J. and Hann, R.: Optimal operation of large agricultural watersheds with water
917 quality constraints, Texas Water Resource Institute, Texas A&M University, Texas, 1978.

918 Wischmeier, W. and Smith, D.: Predicting rainfall erosion losses: a guide to conservation
919 planning, Agricultural Handbook, Science and Education Administration, United States
920 Department of Agriculture, Washington, 1978.

921 Yang, D., Kanae, S., Oki, T., Koike, T., and Musiak, K.: Global potential soil erosion
922 with reference to land use and climate changes, Hydrological Processes, 17, 2913–2928,
923 <https://doi.org/10.1002/hyp.1441>, 2003.

924 Yin, J., He, F., Xiong, Y., and Qiu, G.: Effects of land use/land cover and climate changes
925 on surface runoff in a semi-humid and semi-arid transition zone in northwest China, Hydrology
926 and Earth System Sciences, 21, 183–196, <https://doi.org/10.5194/hess-21-183-2017>, 2017.

927 Zeng, S., Zhan, C., Sun, F., Du, H., and Wang, F.: Effects of climate change and human
928 activities on surface runoff in the Luan river basin, Advances in Meteorology, 6, 1–12,
929 <https://doi.org/10.1155/2015/740239>, 2015.

930 Zhang, F., Shi, X., Zeng, C., Wang, L., Xiao, X., Wang, G., Chen, Y., Zhang, H., Lu, X.,
931 and Immerzeel, W.: Recent stepwise sediment flux increase with climate change in the Tuotuo
932 River in the central Tibetan Plateau, Science Bulletin, 65, 410–418,

933 <https://doi.org/10.1016/j.scib.2019.12.017>, 2020a.

934 Zhang, W., Li, Y., Zhu, B., Zheng, X., Liu, C., Tang, J., Su, F., Zhang, C., Ju, X., and
935 Deng, J.: A process-oriented hydro-biogeochemical model enabling simulation of gaseous
936 carbon and nitrogen emissions and hydrologic nitrogen losses from a subtropical catchment,
937 Science of the Total Environment, 616, 305–317,
938 <https://doi.org/10.1016/j.scitotenv.2017.09.261>, 2018.

939 Zhang, W., Yao, Z., Zheng, X., Liu, C., Wang, R., Wang, K., Li, S., Han, S., Zuo, Q., and
940 Shi, J.: Effects of fertilization and stand age on N₂O and NO emissions from tea plantations: a
941 site-scale study in a subtropical region using a modified biogeochemical model, Atmospheric
942 Chemistry and Physics, 20, 6903–6919, <https://doi.org/10.5194/acp-20-6903-2020>, 2020.

943 Zhang, W., Li, S., Han, S., Zheng, X., Xie, H., Lu, C., Sui, Y., Wang, R., Liu, C., Yao, Z.,
944 and Li, T.: Less intensive nitrate leaching from Phaeozems cultivated with maize generally
945 occurs in northeastern China, Agriculture, Ecosystems & Environment, 310, 107303,
946 <https://doi.org/10.1016/j.agee.2021.107303>, 2021a.

947 Zhang, X., Song, J., Wang, Y., Deng, W., and Liu, Y.: Effects of land use on slope runoff
948 and soil loss in the Loess Plateau of China: a meta-analysis, Science of The Total Environment,
949 755, 142418, <https://doi.org/10.1016/j.scitotenv.2020.142418>, 2021b.

950 Zhou, L., Kaufmann, R., Tian, Y., Myneni, R., and Tucker, C.: Relation between
951 interannual variations in satellite measures of northern forest greenness and climate between
952 1982 and 1999, Journal of Geophysical Research-Atmospheres, 108, ACL 3-1–ACL 3-16,
953 <https://doi.org/10.1029/2002jd002510>, 2003.

954 Zhu, B., Wang, T., Kuang, F., Luo, Z., Tang, J., and Xu, T.: Measurements of nitrate
955 leaching from a hillslope cropland in the Central Sichuan Basin, China, Soil Science Society of
956 America Journal, 73, 1419–1426, <https://doi.org/10.2136/sssaj2008.0259>, 2009.
957

958 Table 1 Performance of the upgraded CNMM-DNDC model in simulating the stream flow,
 959 sediment, and particulate and total nitrogen (N) losses at the Jieliu catchment outlet from 2007
 960 to 2008. Total N refers to the total amount of NH_4^+ , NO_3^- , dissolved organic N and particulate
 961 N.

Variables	Operation	Size	nRMSE	NSI	ULR		
					Slope	R^2	p
Stream flow	Calibration	12	18.29	0.98	0.94	0.96	< 0.001
	Validation	12	34.57	0.89	0.98	0.98	< 0.001
Sediment loss	Calibration	12	34.02	0.94	0.96	0.93	< 0.001
	Validation	12	38.23	0.89	0.90	0.96	< 0.05
Particulate N loss	Calibration	12	49.45	0.87	0.78	0.85	< 0.001
	Validation	12	57.75	0.74	0.92	0.88	< 0.001
Total N loss	Calibration	12	56.98	0.86	1.36	0.98	< 0.001
	Validation	12	42.55	0.86	1.53	0.98	< 0.001

962 The statistical criteria used to quantify the discrepancy between observations and simulations
 963 include the normalized root mean square error (nRMSE), the Nash–Sutcliffe index (NSI) and
 964 the slope, determination coefficient (R^2) and significance level (p) of the univariate linear
 965 regression (ULR). Size represents the sample size. The column “Operation” represents the
 966 evaluation is conducted for model calibration or validation.

967

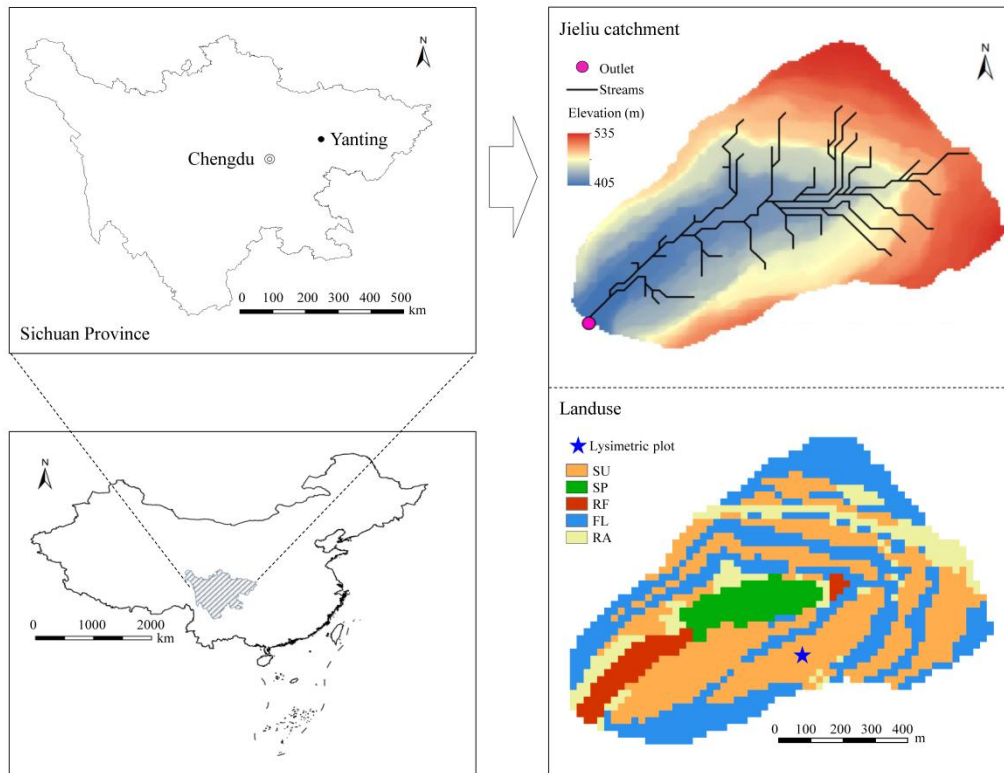
968

969 Table 2 Simulated comprehensive effects of precipitation, air temperature and land use change
 970 on crop yield (Yield), surface runoff, sediment yield, and particulate carbon (C), nitrogen (N)
 971 and phosphorus (P) losses in the validation year of 2008. The low greenhouse gas (GHG)
 972 emission scenario represents the scenario of air temperature increasing by 1.5°C and
 973 precipitation increasing by 10%. The high GHG emission scenario represents the scenario of an
 974 air temperature increase of 4°C and a precipitation increase of 30%. The UFL scenario is the
 975 abbreviation of the scenario of upland change into forest land.

Scenario	Change between the scenario and the baseline (%)					
	Surface runoff	Sediment yield	Particulate C	Particulate N	Particulate P	Yield
Low GHG	21.2	4.1	5.3	5.3	5.3	-6.0
High GHG	72.9	14.8	17.8	18.0	18.1	-16.6
UFL	-12.2	-3.6	-5.6	-7.0	-7.2	-
Low GHG with UFL	5.2	0.2	-0.8	-2.3	-2.5	-
High GHG with UFL	47.9	9.2	9.3	7.8	7.7	-

976

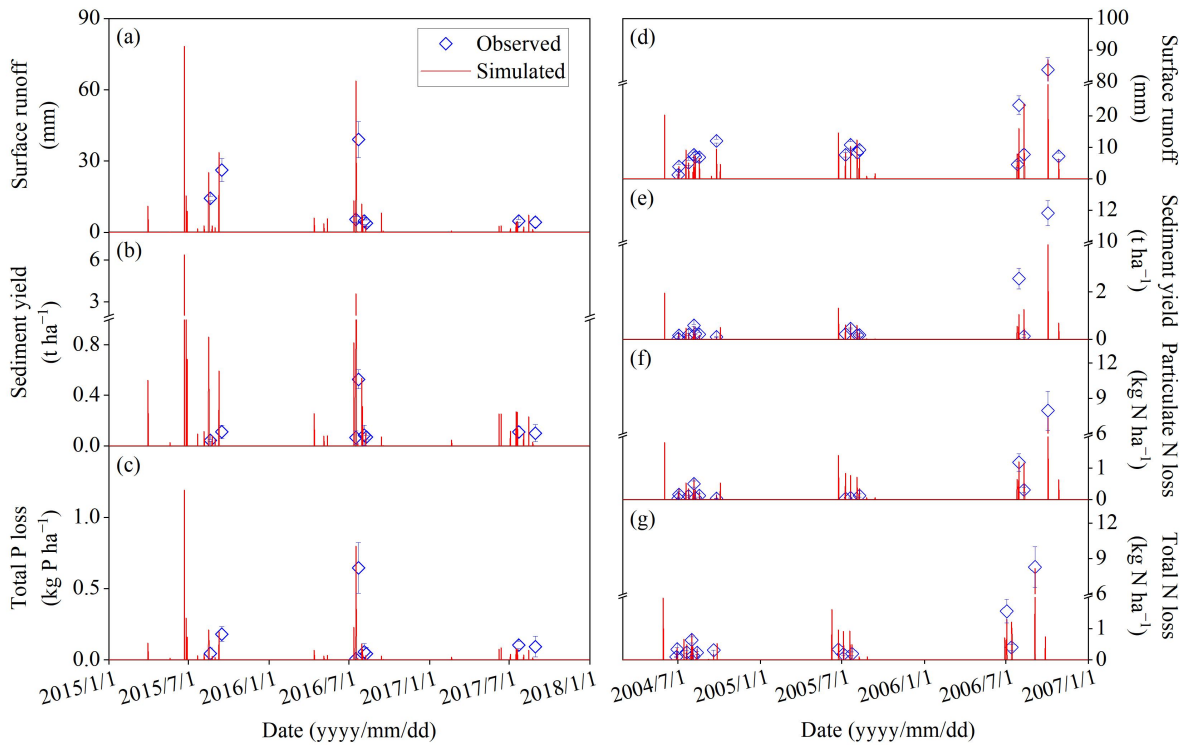
977



979

980 Fig. 1 The location, digital elevation model and land use types of the Jieliu catchment. The land
 981 use types are the sloping uplands (SU) with the summer maize–winter wheat rotation,
 982 seasonally waterlogged paddy (SP) with the paddy rice–winter wheat rotation or paddy
 983 rice–rape rotation, the winter-flooding paddy with the paddy rice-flooding fallow regime (RF),
 984 forest land (FL) and the village residential area (RA).

985



986

987 Fig. 2 Observed and simulated surface runoff (a), sediment yield (b) and total phosphorus (P)

988 losses (c) from 2015 to 2017 and surface runoff (d), sediment yield (e), particulate nitrogen (N)

989 loss (f) and total N loss (g) from 2015 to 2017 in the lysimetric plot. Total P refers to the

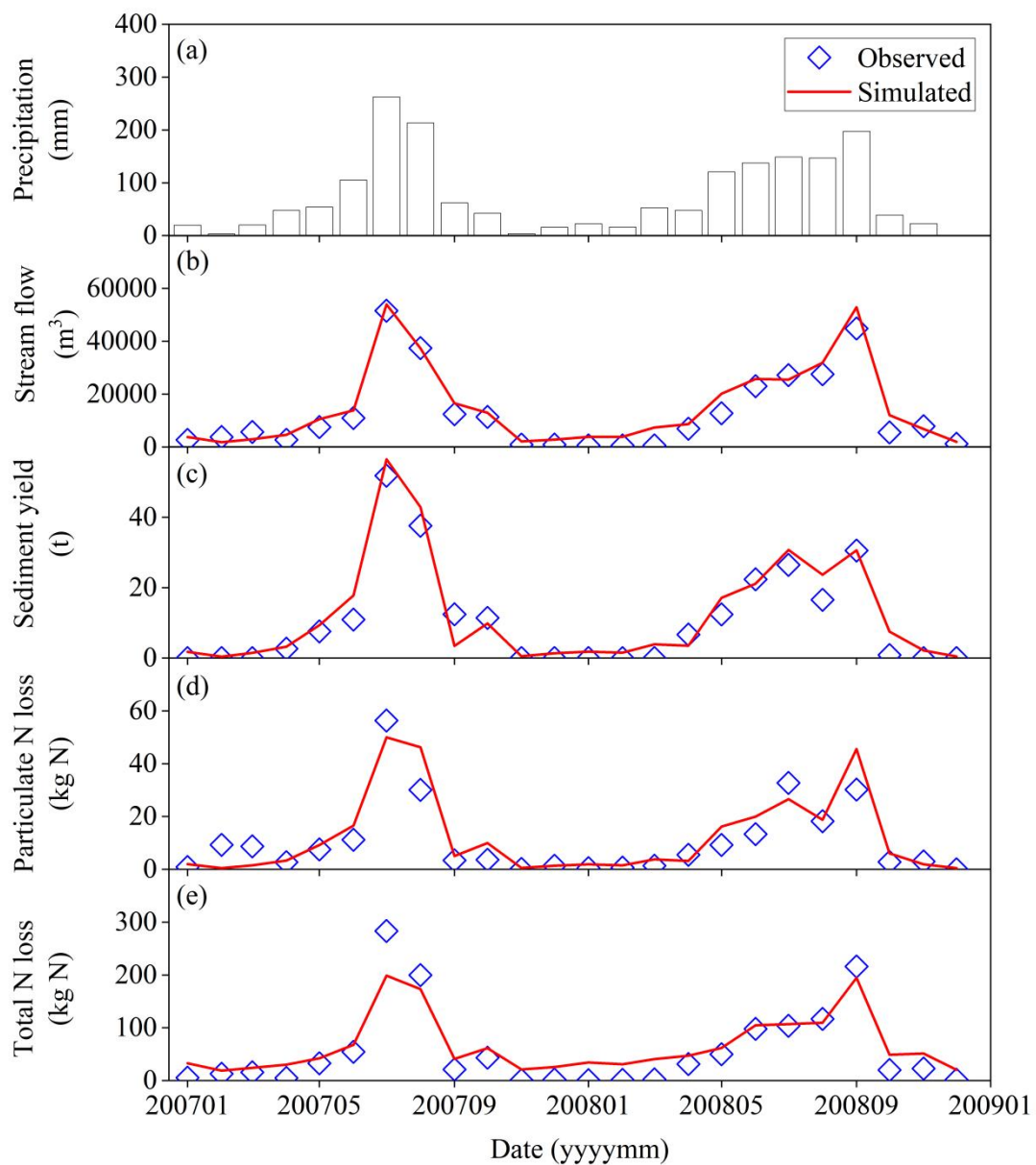
990 dissolved and particulate P. Total N refers to the total amount of NH_4^+ , NO_3^- , dissolved organic

991 N and particulate N. The vertical bars indicate the standard error of three spatial replicates. The

992 observed data cited from Deng et al. (2011), Zhang et al. (2018), Li et al. (2022) and Hu (2020)

993 were provided by Bo Zhu.

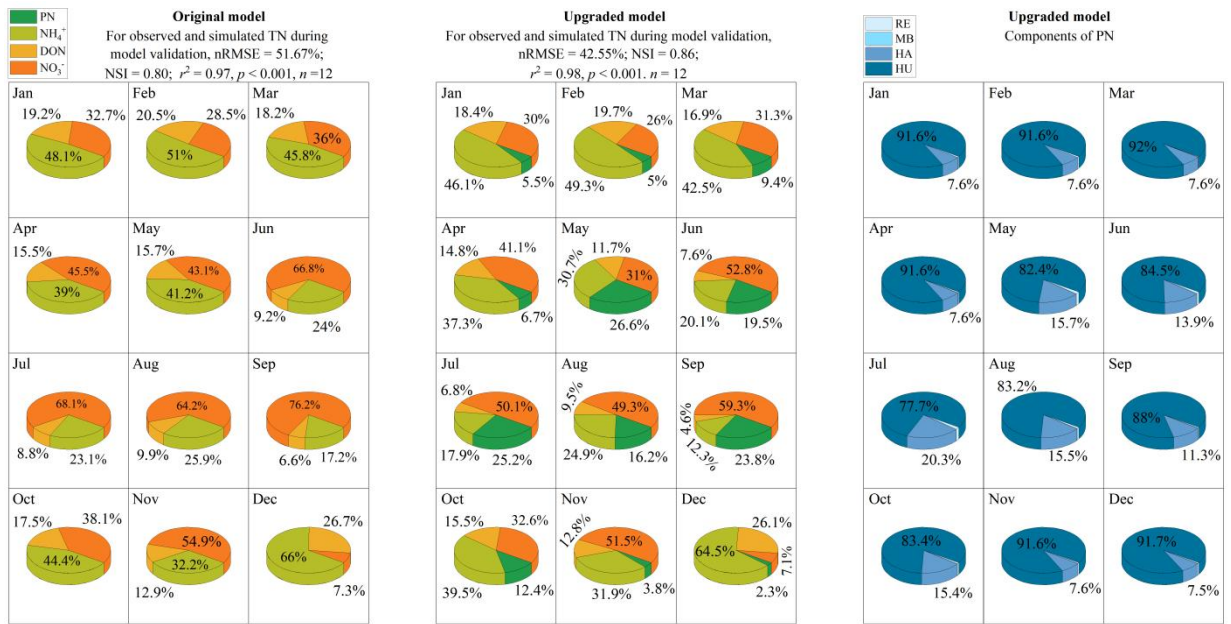
994



995

996 Fig. 3 Monthly observed precipitation (a), observed and simulated stream flow (b), sediment
 997 yield (c), particulate nitrogen (N) loss (d) and total N loss (e) at the outlet of the Jieliu
 998 catchment from 2007 to 2008. Total N refers to the total amount of NH_4^+ , NO_3^- , dissolved
 999 organic N and particulate N. The observed data cited from Deng et al. (2011) and Zhang et al.
 1000 (2018) were provided by Bo Zhu.

1001



1002

1003 Fig. 4 Components of the simulated total nitrogen (TN) of the original CNMM-DNDC and

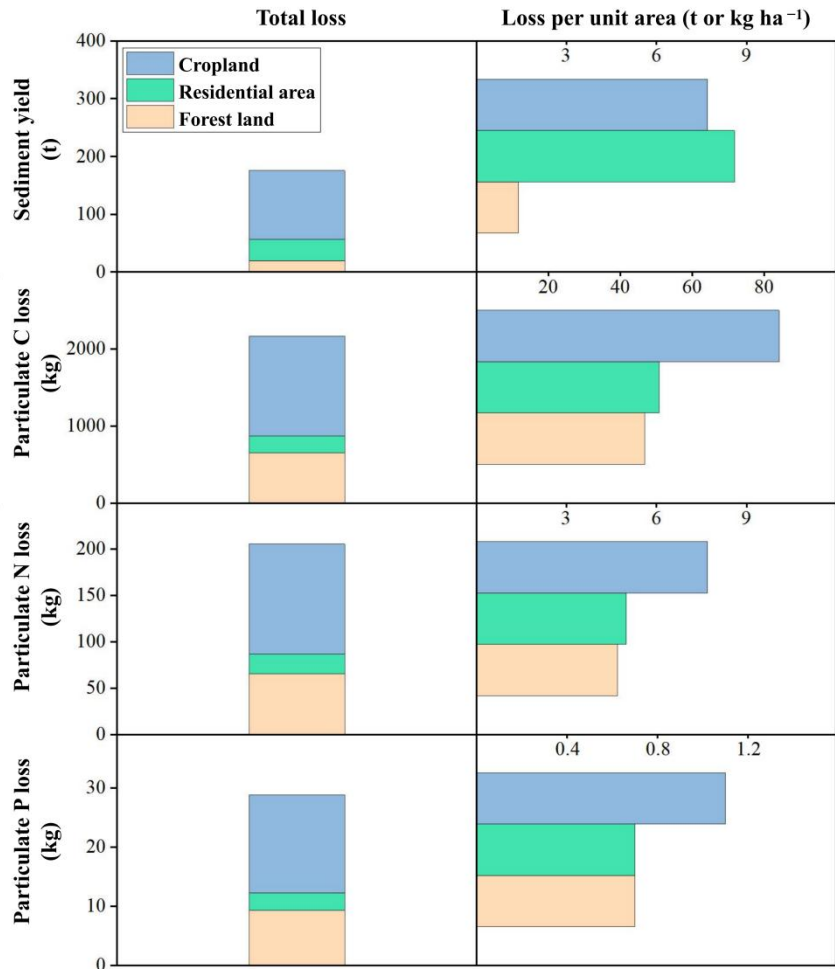
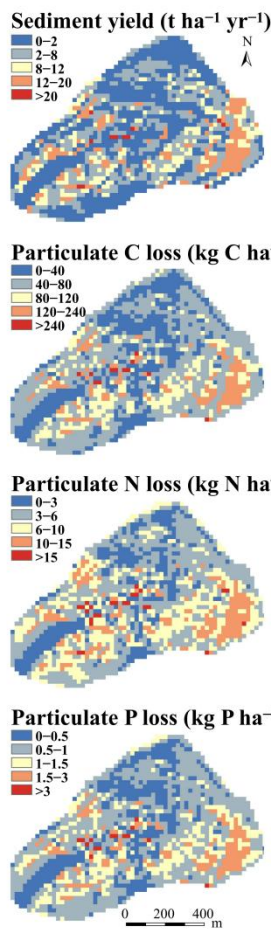
1004 components of the simulated TN and particulate N (PN) of the upgraded model during the

1005 model validation. DON is the abbreviation of the dissolved organic nitrogen. The components

1006 of PN are the N from residue (RE), microbe (MB), labile or resistant humus (HA) and passive

1007 humus (HU).

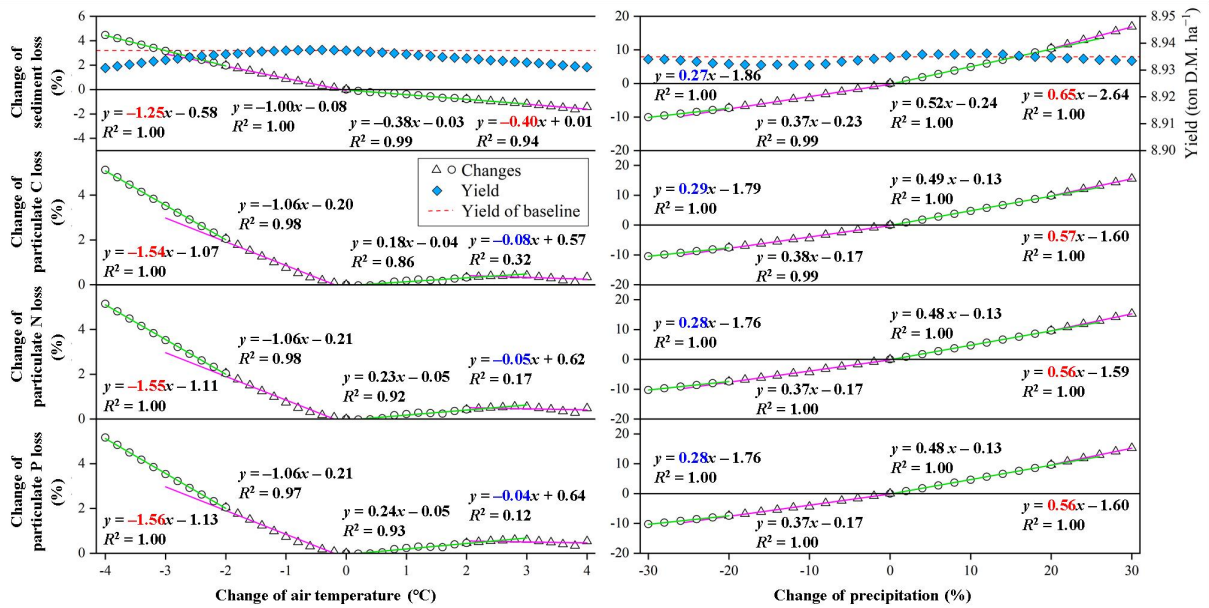
1008



1009

1010 Fig. 5 Simulated spatial distributions of sediment yield, particulate carbon (C), nitrogen (N)
 1011 and phosphorus (P) losses and the effects of different land uses (i.e., cropland, residential area
 1012 and forest land) in the validation year of 2008.

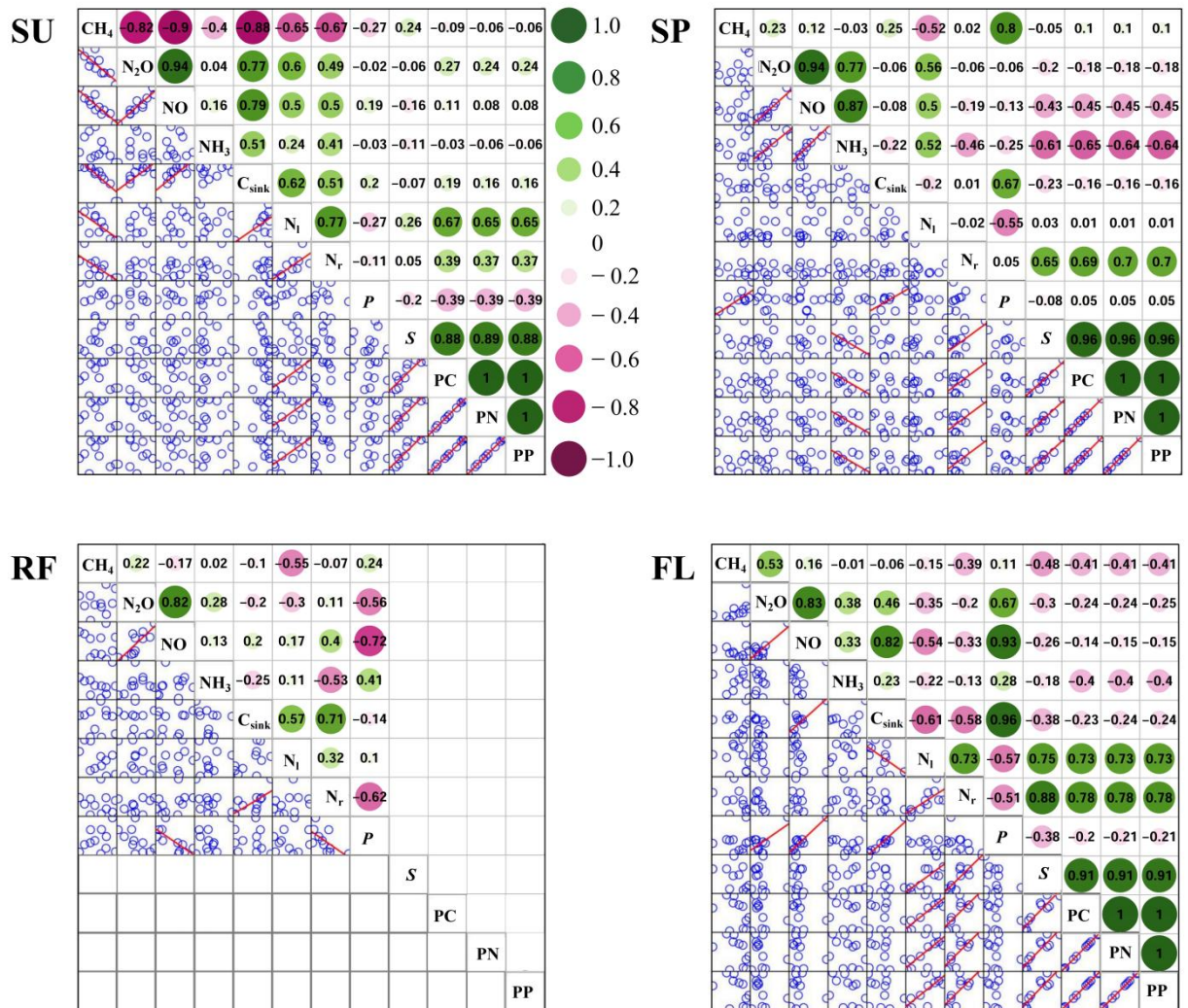
1013



1014

1015 Fig. 6 Simulated effects of precipitation and air temperature change on sediment yield and
 1016 particulate carbon (C), nitrogen (N) and phosphorus (P) losses in the validation year of 2008.

1017 The air temperature and precipitation single-factor scenarios were divided into four sets. The
 1018 scenarios with air temperature reductions and increases 0°C~2°C and greater than 2°C were
 1019 defined as the lower and higher cooling and warming scenarios, respectively. Similarly, the
 1020 scenarios with precipitation reductions and increases 0%~20% and greater than 20% were
 1021 defined as the lower and higher rain-reduced and rain-enhanced scenarios, respectively. The
 1022 numbers in blue and red in front of the letter x represent that the higher warming or cooling
 1023 scenarios (or the higher rain-enhanced or rain-reduced scenarios) result in more and lower
 1024 effects on sediment yield and particulate C, N and P losses than the lower ones, respectively.
 1025 The green and violet lines are referred to the linear regressions between the changes of the
 1026 climate variables (i.e., air temperature and precipitation) and the changes of the variables
 1027 associated to soil erosion. The lines are color-coded to distinguish the results of the different
 1028 scenarios.



1029

1030 Fig. 7 Correlation analysis among the simulated sediment (S), particulate carbon (PC), nitrogen
 1031 (PN) and phosphorus (PP) losses, productivity (P), C sink density (C_{sink}), methane (CH₄),
 1032 nitrous oxide (N₂O), nitric oxide (NO) and ammonia (NH₃) emissions, losses of nitrate through
 1033 leaching (N_i) and surface runoff (N_r) for different land use types. The land use types are the
 1034 sloping uplands (SU) with the summer maize–winter wheat rotation, seasonally waterlogged
 1035 paddy (SP) with the paddy rice–winter wheat rotation or paddy rice–rape rotation, the
 1036 winter-flooding paddy with the paddy rice-flooding fallow regime (RF) and the forest land
 1037 (FL). No losses of S, PC, PN, and PP in the RF crop system because of the year-round flooding
 1038 regime. The figures in the circles stand for the correlation coefficients. The scatter plots of the

1039 bottom left are relating to the correlation coefficients and the linear regression curves (i.e., the
1040 red line) are provided when the correlations with the level of $p < 0.05$ are considered as
1041 significant.